OULUN YLIOPISTO
UNIVERSITY of OULU

DEGREE PROGRMME IN ELECTRICAL ENGINEERING

MASTER'S THESIS

GAS RESPONSE PROPERTIES OF METAL OXIDE NANOPARTICLE BASED SENSORS ON MEMS MICROHOTPLATE PLATFORMS

Author	Tomi Haapalainen
Supervisor	Prof. Jyrki Lappalainen
Second examiner	Prof. Krisztián Kordás
Technical advisor	M.Sc. Joni Huotari

August 2015

Haapalainen T. (2015) Gas response properties of metal oxide nanoparticle based sensors on MEMS microhotplate platforms. University of Oulu, Department of Electrical Engineering, Degree Programme in Electrical Engineering. Master's Thesis, p. 48.

ABSTRACT

This thesis concentrated on the analysis of the gas response properties of several metal oxide based gas sensors. A thin layer of chosen metal oxide was deposited on SGX Sensortech S.A. sensor platforms using pulsed laser deposition (PLD). Metal oxides used in the studies included tungsten trioxide (WO_3), tin oxide zinc oxide (SnO_2-ZnO) and vanadium pentoxide (V_2O_5). The films were deposited at room temperature and various oxygen partial pressures, and were then post-annealed at 400 °C. Gas response measurements were done in two different temperatures and using several gases including nitrogen oxides (NO_x), carbon monoxide (CO), hydrogen (H_2), and ammonia (NH_3). The concentration of the gases were varied during each measurement to probe the sensitivity of the sensors. Gas sensing performance of the sensors were evaluated based on material, selectivity toward different gases, and the effect of surface structure.

Oxygen partial pressure during PLD had a clear impact on the structure of the oxide film. Higher pressure resulted in larger agglomerates of particles, which in general leads to lower gas sensitivity due to factors such as grain size and surface area-to-volume ratio. The measurements showed high responses to NO_x for WO_3 and SnO_2-ZnO samples, as expected. Also, flipping of the response from low concentration to high concentration was observed for WO_3 and SnO_2-ZnO while V_2O_5 showed a mostly stable response.

Key words: gas response, gas sensor, metal oxide, pulsed laser deposition.

Haapalainen T. (2015) Metallioksidinanopartikkeleihin perustuvien kaasuantureiden analysointi MEMS-rakenteissa. Oulun yliopisto, sähkötekniikan osasto, sähkötekniikan koulutusohjelma. Diplomityö, 48 s.

TIIVISTELMÄ

Tässä työssä analysoitiin useiden metallioksideihin perustuvien antureiden kaasuvasteita. Kaasuantureiden substraattina käytettiin SGX Sensortech S.A. valmistamia mikrolämmittimeen pohjautuvia MEMS-rakenteita. Substraatin päälle kasvatettiin ohut kerros valittuja metallioksideja, kuten volframioksidi (WO_3), tinaoksidin ja sinkkioksidin yhdiste (SnO_2-ZnO), ja vanadiumoksidi (V_2O_5). Kasvatusmenetelmänä käytettiin pulssilaserkasvatusta. Kasvatus tapahtui huoneenlämmössä ja useissa eri hapen osapaineissa. Kasvatuksen jälkeen anturit jälkihehkutettiin 400 °C lämpötilassa. Kaasuvastemittaukset suoritettiin kahdessa eri lämpötilassa usealle eri kaasulle, kuten typpioksideille (NO_x), hiilimonoksidille (CO), vetykaasulle (H_2) ja ammoniakille (NH_3). Kaasun konsentraatiota vaihdeltiin mittausten aikana antureiden herkkyyden määrittämiseksi. Kaasuantureiden toimintakykyä arvioitiin materiaalin, selektiivisyyden ja oksidin pintarakenteen perusteella.

Hapen osapaineella pulssilaserkasvatuksen aikana oli merkittävä vaikutus oksidikerroksen rakenteeseen. Suuremmassa paineessa kasvatetut kerrokset muodostivat suurempia partikkeleiden agglomeraatteja, mikä yleisesti ottaen johti heikompaan kaasuvasteeseen johtuen suuremmasta partikkelikoosta ja pienemmästä pinta-alan ja tilavuuden suhteesta. Mittauksissa nähtiin voimakkaita reaktioita typpioksidikaasuihin erityisesti SnO_2-ZnO ja WO_3 näytteiden osalta, kuten oli odotettavissa. SnO_2-ZnO ja WO_3 näytteillä oli myös havaittavissa kaasuvasteen suunnan muutos redusoivasta oksidoivaan kaasukonsentraation kasvaessa, kun taas V_2O_5-näytteet käyttäytyivät enimmäkseen vakaasti.

Avainsanat: kaasuanturi, kaasuvaste, metallioksidi, pulssilaserkasvatus.

CONTENTS

ACKNOWLEDGMENTS

This project has received funding from the European Union's Seventh Framework Programme for research, technological development and demonstration under grant agreement No 604311, Project SENSIndoor.

The author is also very grateful to Dr. Christine Alépée from SGX Sensortech S.A., Switzerland, for providing the MEMS platforms used in the research.

ABBREVIATIONS AND SYMBOLS

AFM	atomic force microscope
FET	field effect transistor
MEMS	microelectromechanical system
MIS	metal insulator semiconductor
PLD	pulsed laser deposition
SCCM	standard cubic centimeter per minute, unit of flow
SCR	selective catalytic reduction
SEM	scanning electron microscope

D, a	grain diameter
D_{avg}	average grain diameter
eV_s	potential barrier
G	conductance
G_0	Richardson coefficient
k	Boltzmann constant
L	depth of depletion (or space-charge) region
$p(O_2)$	oxygen partial pressure
R_a	electrical resistance in air atmosphere
R_g	electrical resistance in gaseous atmosphere
R_q	average surface roughness
$\mathcal{R}$	gas sensor response

Ar	argon
CO	carbon monoxide
CO_2	carbon dioxide
e^-	electron charge
H^+	proton
H_2	diatomic hydrogen gas
H_2O	water molecule
H_2S	hydrogen sulfide
InO	indium oxide
N_2	diatomic nitrogen gas
NO	nitrogen monoxide
NO_2	nitrogen dioxide
NO_2^-	nitrite
NO_x	mixture of nitrogen oxides NO and NO_2
NH_3	ammonia
O^-	oxygen ion
O^{2-}	oxide ion
O_2	oxygen molecule
O_2^-	superoxide

SnO_2	tin dioxide (or tin oxide)
SnO_2-ZnO	tin dioxide zinc oxide compound
V_2O_5	vanadium pentoxide (or vanadium oxide)
WO_3	tungsten trioxide (or tungsten oxide)
ZnO	zinc oxide

1. INTRODUCTION

This thesis concentrated on measuring gas responses of thin film metal oxide nanoparticle gas sensors deposited on SGX Sensortech S.A. MEMS microheater platforms. The films were deposited by pulsed laser deposition (PLD) using various deposition parameters and materials, including WO_3, SnO_2-ZnO, and V_2O_5. The viability of each material toward different gases, including NO_x, NH_3, CO, and H_2 was evaluated through their gas sensing performance and surface property analysis.

Semiconductor gas sensors have been studied for decades ever since the first implications of electrical property changes of tin oxide in a gaseous atmosphere were reported in the 1950's, and as the viability of semiconductor gas sensors were realized [1, 2]. The research has since continued due to the affordable nature and miniature size of this type of gas sensors. Gas sensing is important in many industrial applications such as methane detection in mines, process control, and medical applications, selective catalytic reduction, polluting gas detection from vehicles, and controlling indoor air quality, and environmental monitoring. Research is mostly based on improving three important properties that are sensitivity, selectivity, and stability. Sensitivity refers to the magnitude of change in electrical properties in gaseous atmospheres, selectivity to the ability to react only to specific gaseous stimulants and stability to the repeatability of the sensor reactions over many interactions as in its ability to respond with similar magnitude to each equivalent stimulant, and to recover to its original state after the stimulant is no longer present.

The thesis begins with a short introduction into semiconductor gas sensors followed by basic theory. Theory is applicable to many types of gas sensors, but here the focus was on resistive semiconductor Taguchi-type gas sensors. Sensing mechanisms as well as reactions between specific gases and oxide surfaces are reviewed. Effects of material properties including grain size and catalytic particles in the oxide layer are also discussed. Some parameters important in the performance analysis of gas sensors are described. Pulsed laser deposition, that is the method used to deposit metal oxides on the sensor structures, is also briefly described.

Detailed information on the construction of the samples is given as well as the methods used to measure gas response and other electrical properties of the samples. Measurement processes are also briefly described.

Analysis of surface structure was done by means of X-ray diffraction, Raman spectroscopy, atomic force microscopy (AFM), and scanning electron microscopy (SEM). Data obtained from AFM and SEM analyses are presented with brief notes on X-ray diffraction and Raman spectroscopy results. Current-voltage measurements are presented and briefly analyzed. Results for gas response measurements are discussed in light of surface structure, deposition parameters, and measurement temperature. Selectivity towards specific gases is discussed. An experiment of selective catalytic reduction (SCR) environment was measured for a selected sample to determine cross-sensitivity behavior, and the result is discussed.

2. RESISTIVE METAL OXIDE GAS SENSORS

In the field of semiconductor gas sensors, there are several types of gas sensing devices including resistive, diode, MIS (metal-insulator-semiconductor) capacitor, MIS FET (field-effect transistor), and oxygen concentration cell, which use resistance, bias current, bias potential, threshold voltage and cell voltage as their response signals [3]. This work concentrated on the Taguchi-type resistive semiconductor gas sensors [1]. Furthermore, these sensors can be divided into surface sensitive and bulk sensitive gas sensors. Bulk resistive sensors are generally used at high temperatures while surface sensitive sensors, which this thesis concentrates on, are used at lower temperatures.

Resistive semiconductor gas sensors are based on metal oxides such as tin oxide, copper oxide (CuO), indium oxide (InO), tungsten oxide (WO_3), vanadium oxide (V_2O_5) and zinc oxide (ZnO). Tin oxide can be considered the most widely used and researched of the materials. This thesis concentrated on the *n*-type materials such as previously mentioned WO_3, tin oxide zinc oxide compound (SnO_2-ZnO), and V_2O_5 later to be referred to as tungsten oxide, tin oxide, and vanadium oxide. Different materials have been developed for detecting certain gases. Increasing the sensitivity toward certain gases, that is, selectivity, can also be modified through impurities in the oxide. Some examples of materials for specific gases include WO_3 for nitrogen dioxide, WO_3 with added gold or platinum impurities for NH_3, SnO_2 with ZnO for hydrogen sulfide (H_2S), and many others [4].

Figure 2.1 (reprinted from [5], with permission from Elsevier) shows an example structure of a film based resistive semiconductor gas sensor and an ideal gas response curve. The structure in Figure 2.1 (a) is similar to the one used in the sensors of this thesis with interdigitated electrodes under the oxide layer, and a microheater beneath the electrodes. There are many other types of structures applicable for sensors including a sintered block, a coated tube or a heater coil, and electrodes inserted into a bead.

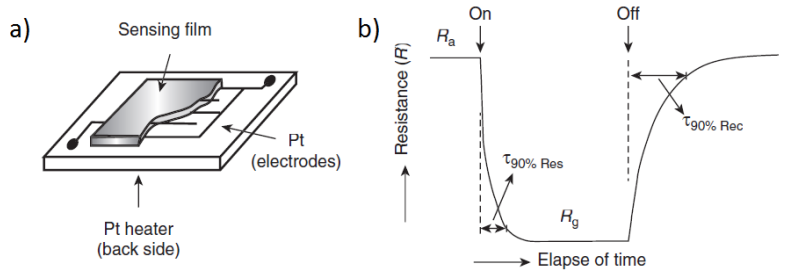

Figure 2.1. (a) Structure of a resistive semiconductor gas sensor. (b) Ideal plot of a sensor's response.

An ideal response of a sensor is illustrated in Figure 2.1 (b), where, in this case, the gas pulse causes a reducing response, that is, a decrease in resistance. R_a denotes the sensor's resistance in air atmosphere and R_g its resistance in gaseous atmosphere. As the gaseous stimulant is introduced, the resistance of the sensor drops rapidly, and given enough time, saturates to a certain level. As the stimulant is removed, the sensor's resistance rises back to its original value. The Figure also shows the definitions for response time and recovery time; response time ($\tau_{90\%\,Res}$) is calculated as the time the sensor takes to reach 90% of its maximum response to the gas, and recovery time ($\tau_{90\%\,Rec}$) as the time the sensor takes to reach 90% of its resistance value in air atmosphere.

3. THEORY

Metal-oxide gas sensor operation is based on adsorption of gas molecules on the surface of the oxide. Adsorbed molecules result in changes in the electrical properties of the oxide. The change in conductivity of a semiconductor in a gaseous atmosphere was first observed by Brattain and Bardeen in 1953 which eventually led to the study of metal oxide gas sensors [6]. Viability of metal oxides as gas detecting elements was first proposed by Taguchi in 1962 and Seiyama *et al.* in 1962 [1, 2], when it was discovered that the gas response of a semiconductor at higher temperatures was much faster, providing a basis for gas sensing utilizing metal oxides. These types of resistive semiconductor gas sensors are commonly referred to as Taguchi-type gas sensors. Metal oxides are feasible for gas sensing applications due to the reversible nature of the gas interaction, that is, the effect of gas on the conductive properties of a metal oxide recover to their original state after gaseous compounds are no longer present.

3.1. Sensing mechanism

At an elevated temperature, between 150 and 500 °C, oxygen adsorbs onto the surface of metal oxides as ions (O_2^-, O^{2-}, O^-) [7]. The adsorbed oxygen may increase or reduce the resistivity of the oxide depending on its type. In *n*-type materials, such as WO_3, the adsorbed oxygen accepts electrons from the material resulting in fewer conducting electrons, which translates to increased resistance. In *p*-type materials the effect is converse. O_2 can bind one or two electrons for operating temperatures below 200 °C and above 200 °C, respectively. The reactions can be divided into reducing and oxidizing reactions by the effect they have on the material. In general, reducing gases reduce the resistance of *n*-type materials and oxidizing gases increase their resistance, and the converse is true for *p*-type materials.

3.1.1. Reducing gases

When a metal oxide interacts with a reducing gas, the electron concentration of the oxide is increased, thus reducing/increasing the resistance of an *n*-type/*p*-type material. Some examples of reducing gases are carbon monoxide (CO), nitrogen monoxide (NO), hydrogen (H_2), and ammonia (NH_3). The amount of electrons in the oxide is increased due to reducing gases removing previously adsorbed negatively charged oxygen atoms.

Carbon monoxide reacts with metal oxides by forming carbon dioxide (CO_2). The reaction is described by equations (1) and (2) [8].

$$2CO + O_2^- \longrightarrow 2CO_2 + e^- \quad (1)$$

$$CO + O^- \longrightarrow CO_2 + e^- \quad (2)$$

The reaction equations (1) and (2) correspond to reactions happening at temperatures below 250 °C and above 250 °C, respectively. The reactions lead to a surplus of electrons in the *n*-type/*p*-type oxide, which reduces/increases its resistance.

Similarly to carbon monoxide, nitrogen monoxide is also a reducing gas. Its reaction with preadsorbed oxygen atoms and molecules lead to the formation of

nitrogen dioxide and free electrons on the oxide surface. Reaction with the oxide surface may be described by equation (3) [9]:

$$NO + O^- \longrightarrow NO_2 + e^- \quad (3)$$

Hydrogen (H_2) adsorbs onto metal oxides by dissociating into two H atoms forming bonds with the surface, which leads to increased electron concentration on the oxide's surface. The reaction equation for H_2 adsorption is [10]:

$$H_2 \rightarrow 2H^+ + 2e^- \quad (4)$$

Equations (5) and (6) are used to describe H_2 reaction with preadsorbed oxygen molecules and atoms [8].

$$2H_2 + O_2^- \rightarrow 2H_2O + e^- \quad (5)$$

$$H_2 + O^- \rightarrow H_2O + e^- \quad (6)$$

Ammonia is also a reducing gas. The three main proposed reaction equations for ammonia are presented in equations (7), (8) and (9) [11, 12].

$$2NH_3 + 3O^- \longrightarrow N_2 + 3H_2O + 3e^- \quad (7)$$

$$2NH_3 + 5O^- \longrightarrow 2NO + 3H_2O + 5e^- \quad (8)$$

$$2NH_3 + 4O^- \longrightarrow N_2O + 3H_2O + 4e^- \quad (9)$$

All reactions with ammonia lead to increase in electrons concentrations in the oxide material resulting in decreased resistance for *n*-type materials and increased resistance for *p*-type materials. This kind of behavior is evidenced in the results section of this thesis.

3.1.2. Oxidizing gases

Oxidizing gases serve as acceptors for electrons on the oxide surface, which leads to increased resistance in *n*-type materials due to diminishing amount of available charge carriers. Oxidizing gases include O_2, NO_2, and CO_2. In the presence of other gases, adsorbed oxygen molecules or atoms are quickly removed from the oxide surface because of chemical reactions with the gases.

Oxygen reaction with metal oxide surface can be described with the following reaction equations:

$$O_2 + e^- \rightarrow O_2^- \quad (10)$$

and

$$O_2 + 2e^- \rightarrow 2O^- \quad (11)$$

Equation (10) describes oxygen adsorption at temperatures below 200 °C and equation (11) at temperatures above 200 °C.

Nitrogen dioxide is an oxidizing gas, and the adsorption process is described by the reaction equation (12) [13].

$$NO_2 + e^- \rightarrow NO_2^- \quad (12)$$

The nitrogen dioxide adsorbs as negatively charged ions, thus binding electrons from the oxide surface resulting in increased electrical resistance. However, more complex reactions may occur depending on temperature and NO_2 concentration as depicted by equations (13) and (14) [9]:

$$NO_2 + O^- \rightarrow NO + O_2 + e^- \quad (13)$$

Equation (13) actually represents a reducing reaction. Here NO_2 reacts with negatively charged preadsorbed oxygen atoms to form nitrogen monoxide, oxygen and free electrons on the material surface.

$$2NO_2 + 2e^- \rightarrow N_2O_4^{2-} \quad (14)$$

This reaction leads to poisoning of the material due to the hard bonding of the doubly charged $N_2O_4^{2-}$ ions. The complex nature of NO_2 reactions combined with the reactions of NO cause the erratic behavior of NO_x response displayed in measurement results.

Carbon dioxide has several ways of interacting with metal oxides such as through reactions with preadsorbed hydroxide, preadsorbed protons, and surface electrons and forming carbonate ions [8]. Carbonate ions are formed with preadsorbed oxygen ions according to equation (16).

$$CO_2 + O^{2-} \rightarrow CO_3^{2-} \quad (15)$$

Oxidizing gases tend to have similar reactions with the oxide surface either by trapping free electrons or combining with preadsorbed oxygen atoms or molecules.

3.1.3. Energy band properties

As oxygen ions and other molecules adsorb onto metal oxides, they cause either electrons to be trapped in them or being supplied into the oxide. This, in turn, causes energy band bending of the material [5]. Molecules that adsorb onto the surface of an oxide can donate electrons to the oxide if the highest occupied orbitals of the molecule are higher than the Fermi level of the oxide. The adsorbed molecules can also behave as acceptors for electrons if the lowest unoccupied molecular orbitals of the adsorbate are below the Fermi level of the oxide. In Figure 3.1 (reprinted from [14], with permission from Elsevier), there is presented an energy band diagram of a clean *n*-type metal oxide surface layer. Net negative charge on the oxide surface causes an electric field in the surface. The field causes bending of the energy bands upwards forming a zone depleted of electrons. In the case of *p*-type metal oxide surface, the bands would instead bend downward leading to a reversed effect.

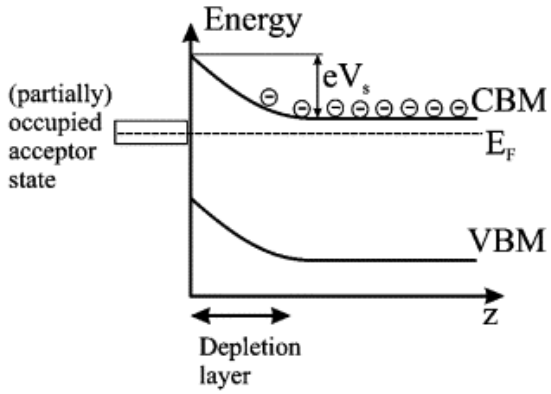

Figure 3.1. Schematic representation of band bending at the surface of a material.

Band bending is also present at inter-granular level; every grain is surrounded by a depletion region due to reconstruction layer, and adsorbed atoms or molecules. The situation, in the case of negatively charged oxygen atoms, is depicted in Figure 3.2 (reprinted from [14], with permission from Elsevier). Similarly to the situation on the material surface in Figure 3.1, the negatively charged oxygen atoms cause an extra upward band bending in the conduction and valence bands in the grains, which is seen as a potential barrier eV_s.

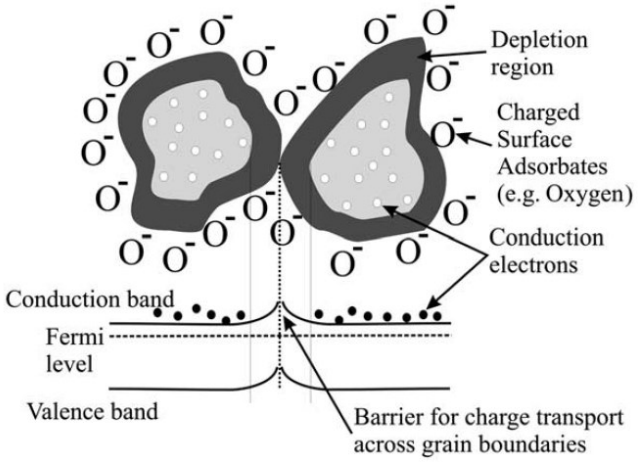

Figure 3.2. Schematic representation of Schottky-like barrier formation between, for example two SnO_2-ZnO grains with adsorbed oxygen atoms.

Electrons moving from grain to grain must therefore overcome a potential barrier of eV_s. The basic concept of conductance in the inter-granular contact can be described simply by equation (16) [15]:

$$G = G_0 exp(-\frac{eV_s}{kT}) \tag{16}$$

where G_0 is the Richardson coefficient, k is the Boltzmann constant, and T is temperature. This equation, however, is only applicable at temperatures where all donors may be considered ionized and hole concentration can be ignored.

3.2. Material properties

Gas sensing properties of a material are strongly influenced by microstructural factors including grain size, surface area-to-volume ratio, porosity, film thickness, surface and sensor geometry, etc. Increasing the reactive surface area of the material greatly improves the sensing properties. Having a large surface area compared to the bulk volume increases chemical reaction area, which affects the electrical properties of the material, making the response higher and often faster compared to a low surface area-to-volume ratio material. Surface area-to-volume ratio may be controlled through adjusting the porosity, film thickness, and grain size of the material. By controlling deposition parameters, for example oxygen partial pressure ($p(O_2)$) during PLD, these parameters may be optimized.

3.2.1. Grain size

Grain size of the material has a profound effect on the gas sensing properties of a semiconductor. It has been shown that gas response is strongly dependent on the relationship of grain size, diameter D, and depth of the depletion (or space-charge) region L [16, 17]. In this work gas response is defined as the ratio of change of resistance from air atmosphere to gaseous atmosphere $R_g - R_a$ and resistance in air R_a in percentages:

$$\mathcal{R} = \frac{R_g - R_a}{R_a} \cdot 100\% \tag{17}$$

Decreasing the grain size close to the value of 2L, or below, increases sensitivity drastically. Comparable effect can be achieved by decreasing the depletion region depth by adding impurities to the crystal structure of the material.

Figure 3.3 illustrates the effect of grain size on conduction model with respect to the ratio of grain diameter and depletion region depth (reprinted with permission from [18], Copyright 2004, AIP Publishing LLC). In the region where grain size is much larger than twice the depletion region depth, conduction is controlled by grain boundaries. In this model individual grains are connected by necks and form larger agglomerates that are connected to other agglomerates of grains by grain boundaries, as in Figure 3.3 (a). As the core region is the main path of conduction, gas atoms or molecules adsorbed onto the surface will not have a great effect on conduction at grain sizes much larger than twice the depletion region depth.

When the grain size starts to decrease close enough to twice the depletion region depth, the dominating conduction model are necks between grains, as shown in Figure 3.3 (b). In this region the depth of the depletion region pushes much farther into the grains thus causing the core region of the grains to reduce in size and therefore become less capable of charge transfer. Thus, larger surface area-to-volume ratio is more sensitive to measured gas.

As the grain size decreases below that of twice the depletion region depth, conduction is diminished because the depletion region covers the entire grain rendering it completely free of charge carriers. It is in this region that gas sensitivity has been reported to be the highest [17]. This is because the charge density modulation, and thus the modulation of conductivity is solely caused by reaction due to adsorbed surface ions and molecules.

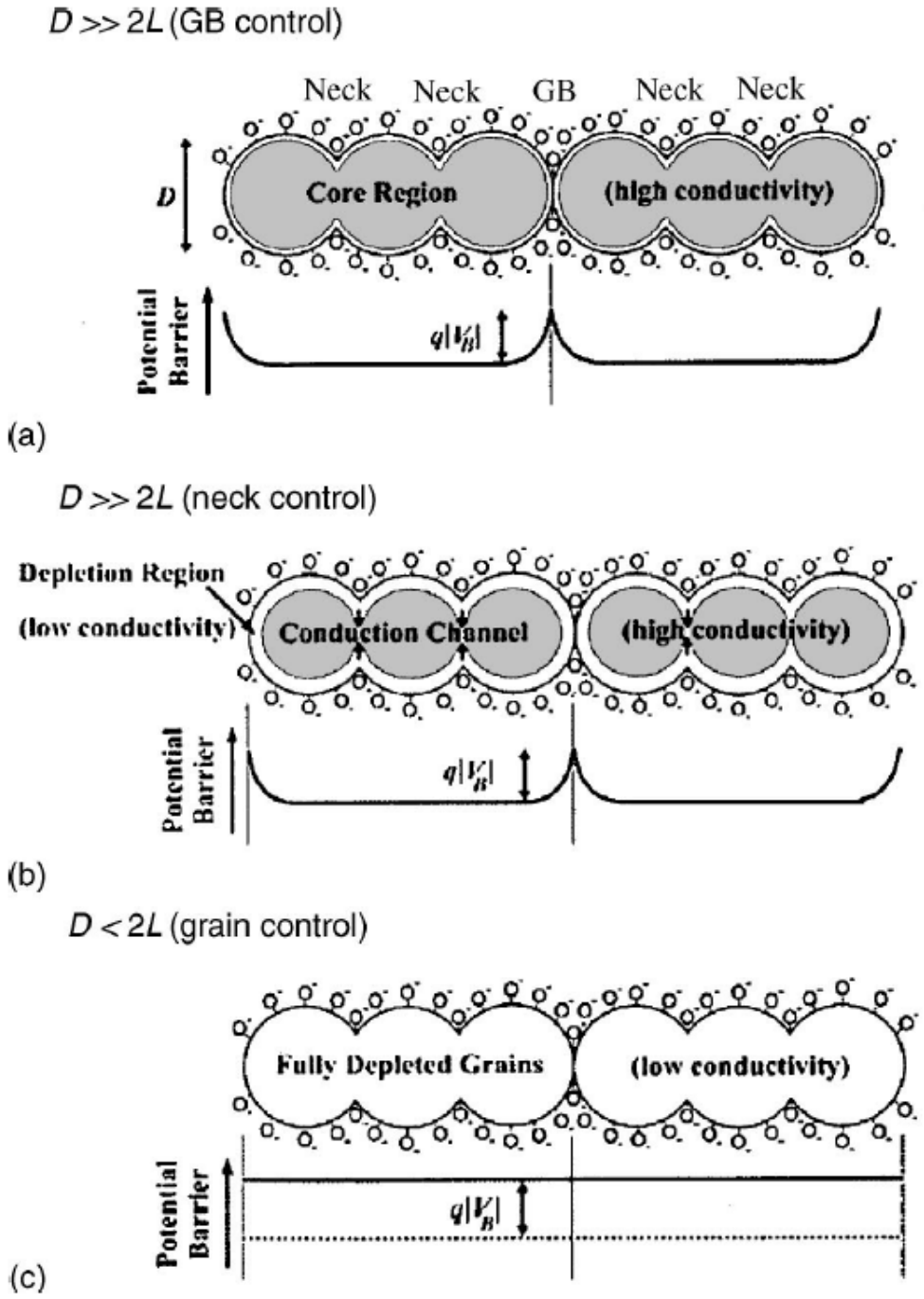

Figure 3.3. Model of the effect of crystallite size on the sensitivity of a metal oxide gas sensor. (a) D >> 2L, (b) D ≥ 2L and (c) D < 2L.

Thus, gas sensitivity is related to grain size through the proportionality $1/D_{avg}$, that is, inverse relation to average grain diameter. Generally, the smaller the grain the better the sensing properties. A critical limit to grain size has been observed, where gas sensing properties of the material will start to increase rapidly with smaller grains [19]. Figure 3.4 shows the calculated dependence of potential barrier height between grains on grain diameter (reprinted from [19], with permission from Elsevier).

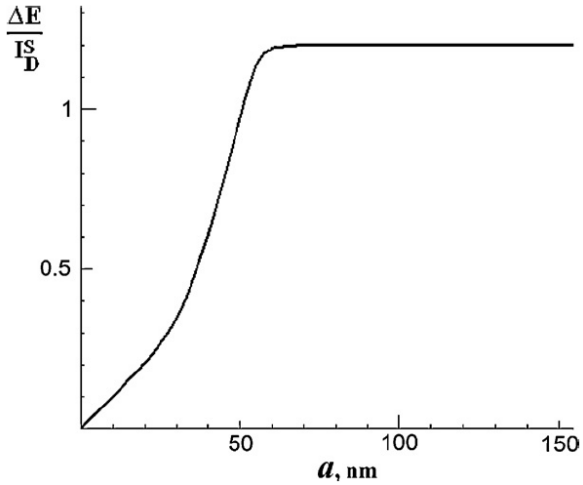

Figure 3.4. Dependence of potential barrier height ΔE on grain diameter a = D.

The Figure shows a rapid decline of potential barrier height after a certain grain size is achieved. The critical limit for grain size was determined to fall in the range of 80 – 100 nm. Below this point the amount of conduction electrons was determined to drop drastically resulting from the effect named as charge carrier self-exhaustion of the material, that is, the disappearance of the capacitor-like double layer of charge carriers on the material surface at sufficiently small grain sizes [19]. However, there is a lower limit to grain size, in the scale below 10 nm, after which sensitivity does not increase anymore.

3.2.2. Catalytic modifications

Small amounts of noble metals such as gold, platinum, or palladium can be added to metal oxides to improve their sensitivity, selectivity, and response time towards a particular gas. Other catalytic modifiers include various other metals and their oxides. Catalytic modifiers have been used to achieve responses towards complex gases and for improving overall selectivity. The mechanism of additives can be divided into electronic and chemical reaction according to the way they interact with the oxide [16]. Table 1 (reprinted from [16], with permission from Elsevier) illustrates the mechanisms of electronic and chemical sensitization for a noble metal loaded SnO_2-ZnO sensor.

Table 3.1. Chemical and electronic sensitization in noble metal loaded SnO_2-ZnO

Type	Chemical	Electronic
Model	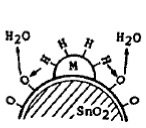	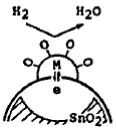
Role of noble metal	Activation and spill-over of sample gas	Electron donor or acceptor
Origin of gas-sensitive properties	Change of adsorbed oxygen concentration	Change of oxidation state of noble metal
Example	$Pt-SnO_2$	Ag_2O-SnO_2, $PdO-SnO_2$

In chemical sensitization, the noble metals accelerate the chemical process which leads to reduced concentration of adsorbed oxygen on the surface of the oxide. Therefore it does not directly impact the gas sensing mechanism of the metal oxide, but instead promotes chemical processes on the oxide surface.

In electronic sensitization, the noble metals shift the work function, that is, the minimum required energy to remove an electron from a solid to a point in the vacuum immediately outside the solid. Noble metals that interact with oxides by electronic sensitization can form stable oxides in air atmosphere. In the presence of an inflammable gas, these oxides are easily reduced to metals.

3.3. Parameters

Gas sensors are characterized by several parameters including sensitivity, selectivity, stability, response time and recovery time. These parameters can be depicted in various ways.

Response of Taguchi type gas sensor is often described as the ratio of resistance in gas atmosphere and resistance in air atmosphere. In this study, gas response is depicted as the ratio of change of resistance in gas to resistance in air in percentages, as described in equation (17).

Selectivity means the sensor's ability to react only to specific gaseous atmospheres. Selectivity of a gas sensor is an important property in many applications from air quality control to industrial processes such as selective catalytic reduction (SCR), in which nitrogen oxides are converted into diatomic nitrogen and water using a gaseous reductant such as ammonia or urea. Different materials and sensitizers are used to achieve selectivity to certain gases, for example WO_3 is generally regarded as a strong NO_x sensor while showing a much lower sensitivity towards gases like NH_3, CO, and H_2.

The stability of gas sensors is also important for long-term use and reliability. Thin film based gas sensors traditionally suffer from lack of stability due to the porous structure of the film being compromised by heating and poisoning from gases. Thick film based sensors are more stable, but response is generally much lower due to gases affecting only the surface of the film while electrical conduction mostly occurs in the bulk.

In the case of toxic gases such as carbon monoxide, response time of the sensor becomes important. Response time refers to the sensor's ability to alter its electrical properties in as short time as possible in gaseous atmosphere with respect to gas concentration. Response time is usually defined as the time the sensor's resistance requires to change from its ambient value, i.e. resistance in air, to the point where 90% of resistance change from air atmosphere to gas atmosphere has been achieved. To lesser extent, recovery time of a gas sensor is also important; the sensor must be able to recover to its ambient state in sufficient time after the gaseous stimulant has been removed.

Research done in the field of semiconductor gas sensors aims to optimize these (and other) parameters. Depending on the application, some parameters may become more important, but in general, a good compromise between parameters is the best choice.

3.4. Pulsed Laser Deposition

Pulsed laser deposition (PLD) refers to the use of a high-power laser pulses to deposit thin film materials. The technique was first presented by Smith and Turner in 1965 [20]. Due to various other thin film deposition methods such as sputtering and molecular beam epitaxy, and sporadic research done on the method led to the technique resurfacing only in the late 1980's [21]. Popularity of the method has steadily risen due to its simplicity, versatility, and cost-effectiveness in depositing thin-film materials.

The basic idea of pulsed laser deposition is simple; target material is vaporized by the laser in a vacuum chamber, and is deposited on a substrate facing the target material. Rapid heating of the target material causes the formation of an ablation plume which contains, for example, molecular fragments, ions, and neutral particles. The deposited layer is affected by the wavelength of the laser, energy density and duration of the laser pulse. In PLD, the laser is commonly operated at the 200 – 400 nm wavelength range.

In recent years pulsed laser deposition has been used extensively in the deposition of a myriad of materials including ZnO nanowires [22], CZTS (copper zinc tin sulfide) thin films for solar cells [23], pure and Ag doped SnO_2-ZnO thin films [24], and many others. The growth in popularity of the method can be credited to the simplicity of the setup, the fact that the deposition conditions can be varied in a broad range, and a large number of materials can be deposited using this technique.

Especially in the case of metal oxides, PLD is generally the most versatile fabrication method for thin films and nanostructures. This is due to ease of controlling and repeating the chemical composition and stoichiometry of the studied target material in thin films and nanostructures. Also, the materials with extremely high melting and evaporation temperatures can be easily processed by the PLD method.

4. EXPERIMENTS

All sensors used in the measurements were deposited on SGX Sensortech S.A. MEMS microelectromechanical system microheater platforms. SGX Sensortech is a partner, along with Functional Electroceramics Thin Film (FETF) group of the Microelectronics and Material Physics Laboratories in the University of Oulu, and several others, in the European Union FP7 framework project SENSIndoor which aims at development and research of novel gas sensors for control of indoor air quality.

4.1. Sample preparation and instruments

The sensors were constructed on a silicon substrate with a microheater placed under interdigitated electrodes. The structure of a die containing two sensors is shown in Figure 4.1. Metal oxide layers were deposited on the sensors using pulsed laser deposition (PLD). Metal oxides used as the sensing material were WO_3, V_2O_5, SnO_2-ZnO, and SnO_2-ZnO with added platinum particles.

The PLD was conducted using Lambda Physik Compex 201 excimer laser with wavelength of 308 nm and repetition rate of 5 Hz. The depositions were done at room temperature. After deposition, the samples went through a post-annealing process at 400 °C. Several different oxygen partial pressures were used during the deposition process including 0.08 and 0.2 mbar for WO_3, 0.04, 0.1, and 0.2 mbar for V_2O_5, and 0.08 and 0.2 mbar for SnO_2-ZnO and 0.1 mbar for SnO_2-ZnO with added platinum. The fluence of the laser pulses for all samples was 1.25 J/cm^2.

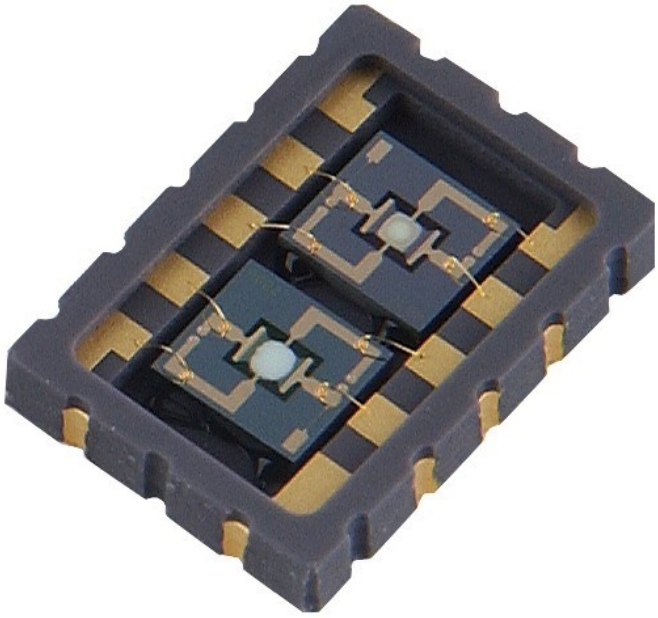

Figure 4.1. Die containing two sensors with light gray oxide layers seen in the middle of the structures.

Conductivity measurements were carried out by using a Keithley 2612A System Source Meter for measuring current and a HP 6626A System DC Power Supply for providing DC current for the sensor heater. A HP 3458A Multimeter was utilized for resistance measurement during gas measurements. Gas measurements were done using a Linkam THMSE600 measurement stage and chamber set at room temperature during the measurements. The chamber used for the gas measurements can be seen in Figure 4.2.

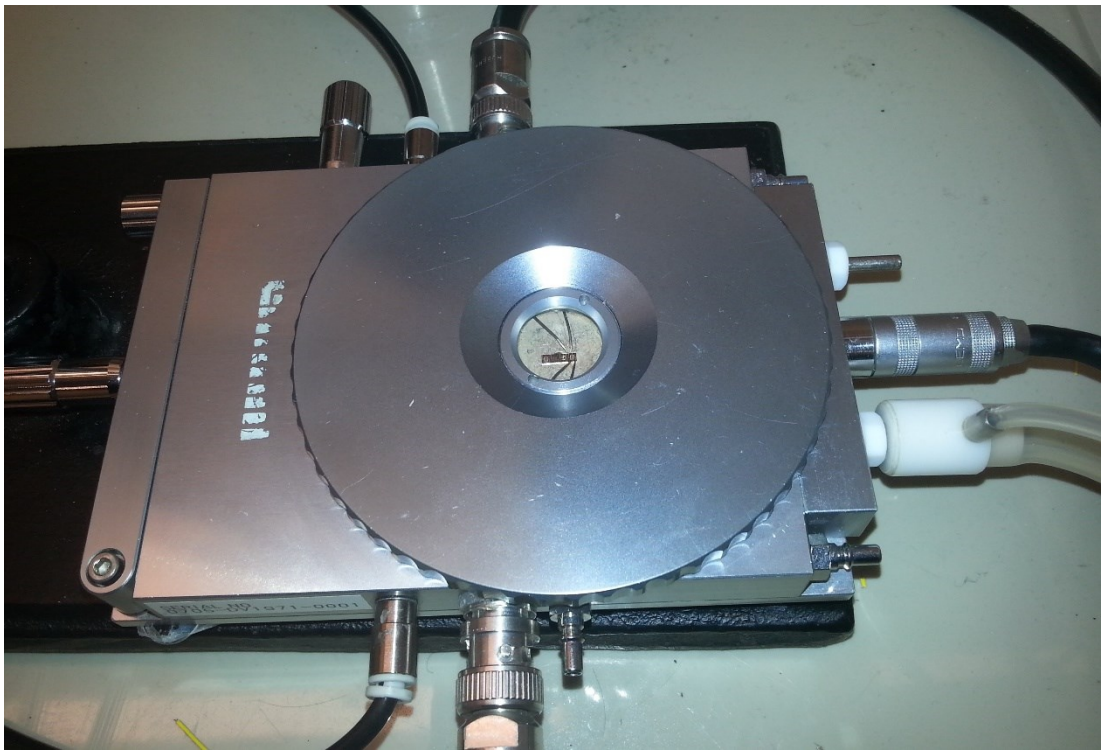

Figure 4.2. Linkam THMSE600 measurement stage with a chip containing four sensor samples in the measurement chamber.

4.2. Measurements

Measurements were done using the microheater integrated into the sensor structure electrodes as the source of heat. The temperature of the heater was controlled by varying the voltage applied to it. Temperatures of 200 °C and 350 °C of the heater were used in the measurements. The temperatures correspond to approximately 40 mW and 72 mW power consumption in the heater, which were achieved by applying a voltage of 1.6 V and 2.3 V, respectively. Sensors were subjected to air flow and heating before introducing gases into the measurement chamber. The air flow was kept as low as possible to achieve desired concentrations for the gases without causing extra cooling to the sensor. After the heating period in synthetic air flow, gases were introduced in 15 minute pulses with increasing concentration, and 15 minute pulses of synthetic air between the pulses. A longer period of synthetic air flow was introduced between different gases.

Gases used in the measurements included NO_x, NH_3, CO, or H_2 in argon with synthetic air as carrier gas. Synthetic air used as the carrier gas composed of 80% nitrogen (N_2) and 20% oxygen (O_2). Measurement gases composed of 100 ppm NO_x,

50 ppm NH_3, 1000 ppm CO each in N_2, and 10 000 ppm H_2 in Ar as initial source concentrations. Concentrations used for different gases in the measurements were as follows; 2, 5, 10, 20, 30, and 50 ppm for NO_x, 3, 5, 10, and 20 ppm for NH_3, 10, 20, 50, and 100 ppm for CO and 70, 90, 140, and 200 ppm for H_2. Gas flow in the measurement chamber was held at approximately 200 standard cubic centimeters per minute (SCCM). The synthetic air flow was lowered accordingly when measurement gases were introduced into the gas flow.

Conductivity measurements were carried out using the same setup as described before with the exception that a source meter was used to measure the current. Measurements were done at room temperature, 200 °C, and 350 °C. Sensors were held at the measurement temperature for approximately two minutes before the measurement. Current was measured using a loop of ±5 V at room temperature, and ±3 V at 200 °C and 350 °C beginning from 0 V going to 5 V or 3 V and back to 0 V followed by -5 V or -3 V and finally returning to 0 V. Voltage was altered in steps of 20 mV. The loop was measured twice, and the second loop is presented in results.

5. RESULTS

Gas sensors were also characterized by studying the surface and microstructure of the materials with several methods including X-ray diffraction, Raman spectroscopy, atomic force microscopy (AFM) and scanning electron microscopy (SEM). Electrical properties of the sensors were evaluated through current-voltage measurements. Gas responses were thoroughly analyzed and compared to surface microstructure observations with emphasis on nitrogen oxides and ammonia. Materials were compared with respect to their responses to measured gases. The selective behavior of some materials towards certain gases are also presented. A practical example of the feasibility of V_2O_5 thin-film sensor for atmospheric control in selective catalytic reduction process (SCR) is evaluated.

5.1. Surface and microstructure characterization

Surface microstructure of the samples were studied with X-ray diffraction, Raman spectroscopy, AFM and SEM. X-ray diffraction and Raman spectroscopy were used to determine phase structure of the metal oxides, and the results are only briefly discussed. AFM and SEM micrographs were acquired to observe the formation of nanoparticles and agglomerates for different deposition parameters.

WO_3 samples were investigated with X-ray diffraction and Raman spectroscopy. Using Raman spectroscopy it was found, that in the 0.08 mbar-samples γ-phase of the material was dominant while both γ- and ε-phase were present in the 0.2 mbar sample. However, X-ray diffraction of the samples revealed that both phases were almost equally present in the $p(O_2)$ = 0.08 and 0.2 mbar samples. This difference may have risen from the fact that Raman spectroscopy concentrates on a smaller area, which may have had a low concentration of ε-phase WO_3. This leads to the conclusion, that performance towards gas sensing is mostly affected by the grain size of the material instead of the presence of specific phases, as confirmed by gas measurements done for the samples. In some experiments, however, the γ-phase WO_3 has been found to be especially responsive to NO_x gas [25].

Figure 5.1 shows the AFM micrographs obtained from both WO_3 samples used in the measurements. Average surface roughness R_q for the 0.08 mbar WO_3 sample was 5.5 nm in comparison to 42.0 nm for the 0.2 mbar sample.

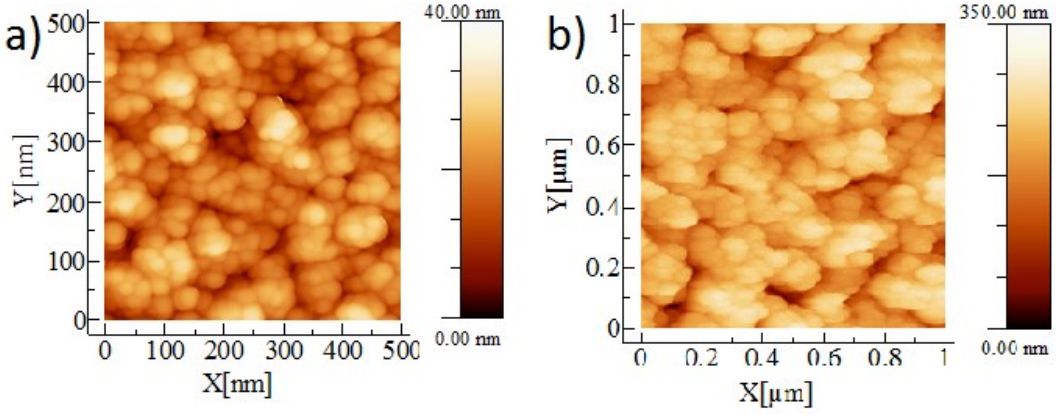

Figure 5.1. AFM micrographs of WO_3 samples deposited in (a) $p(O_2)$ = 0.08 mbar, and (b) $p(O_2)$ = 0.2 mbar.

It is clear from the AFM micrographs that higher oxygen partial pressure during PLD leads to larger agglomerates of particles in the samples. As previously explained, smaller grain size increases response to gases which is also evident in gas measurement results.

Similar properties of the surface structures of SnO_2-ZnO samples shown in Figure 5.2 and V_2O_5 samples shown in Figure 5.3 are also observable. Higher oxygen partial pressure created larger agglomerates on the material surface. Of the SnO_2-ZnO samples, the sensor prepared in p(O2) = 0.2 mbar during PLD, showed the lowest response to almost all studied gases. The other samples, while prepared in similar oxygen partial pressure, had the difference of added platinum particles in the sample. These catalytic particles improved the gas response of the material.

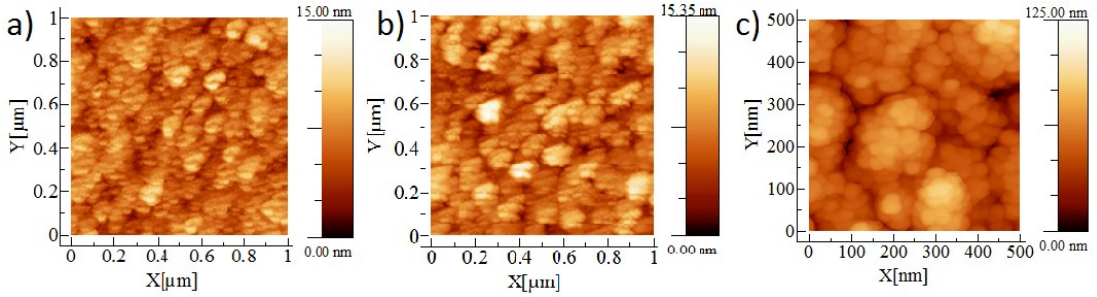

Figure 5.2. AFM micrographs of SnO_2-ZnO samples deposited in (a) $p(O_2)$ = 0.08 mbar, (b) $p(O_2)$ = 0.1 mbar (sample with added platinum), and (c) $p(O_2)$ = 0.2 mbar.

Average surface roughness R_q for the samples were 2.8, 3.4, and 14.1 nm for the 0.08, 0.1, and 0.2 mbar samples, respectively.

AFM micrographs for the V_2O_5 samples are shown in Figure 5.3. Similarly to SnO_2-ZnO samples, the V_2O_5 prepared in the highest oxygen partial pressure had the most porous structure as shown in Figure 5.3 (c). The 0.04 mbar samples showed slight orientation in its grain structure. The R_q for the 0.04, 0.1, and 0.2 mbar samples were 2.7, 2.9, and 8.2 nm, respectively. While the difference between the 0.04 and 0.1 mbar samples was small, the leap from the 0.1 mbar sample to 0.2 mbar was substantial.

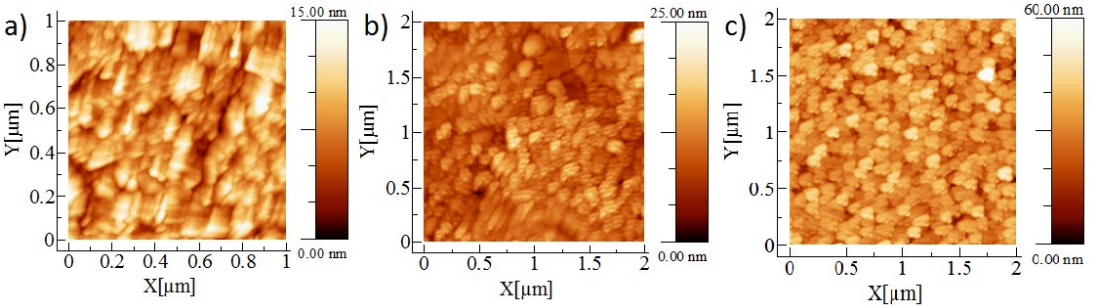

Figure 5.3. AFM micrographs of V_2O_5 samples deposited in (a) $p(O_2)$ = 0.04 mbar, (b) $p(O_2)$ = 0.1 mbar, and (c) $p(O_2)$ = 0.2 mbar.

Generally, the AFM micrographs showed the dependence of agglomerate size and R_q to oxygen partial pressure used in PLD. With increased $p(O_2)$ the agglomerate sizes and R_q increased. Agglomerate sizes were generally approximately 100 nm in diameter.

SEM micrographs were also acquired to study the surface structure and cross-section of some samples. Figure 5.4 shows cross-section micrographs of WO_3 and

V_2O_5 samples, and Figure 5.5 shows corresponding micrographs of SnO_2-ZnO samples. WO_3 and V_2O_5 sample prepared in $p(O_2)$ = 0.2 mbar both showed a highly porous structure suitable for gas detection. The 0.1 mbar V_2O_5 sample had a somewhat more uniform structure which may not be as reactive to some gases as a more porous structure could be.

SnO_2-ZnO samples presented a curious tree-like structure especially for the 0.2 mbar-sample and the 0.1 mbar-sample with added platinum. This kind of structure has a high surface area-to-volume ratio which promotes responsiveness in gas sensing.

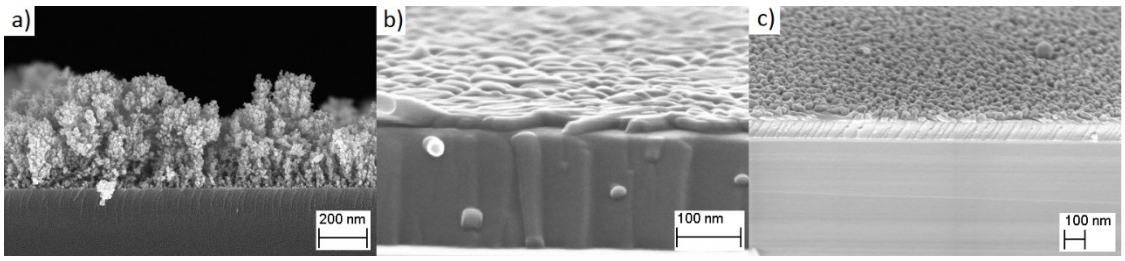

Figure 5.4. SEM cross-section micrographs of (a) WO_3 prepared in $p(O_2)$ = 0.2 mbar and V_2O_5 samples prepared in (b) $p(O_2)$ = 0.1 mbar and (c) $p(O_2)$ = 0.2 mbar.

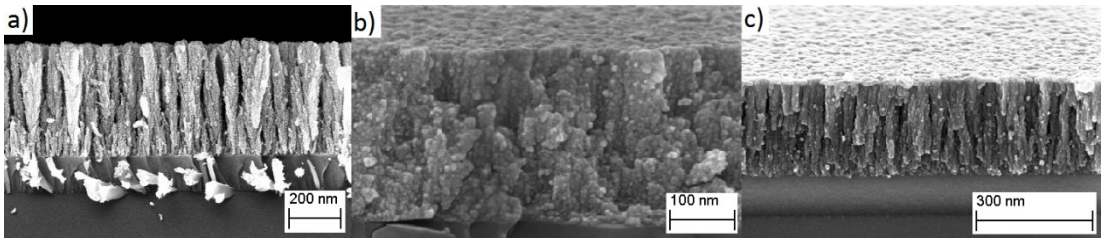

Figure 5.5. SEM cross-section micrographs of SnO_2-ZnO samples prepared in (a) $p(O_2)$ = 0.2 mbar, (b) $p(O_2)$ = 0.08 mbar, and (c) SnO_2-ZnO sample with added platinum prepared in $p(O_2)$ = 0.1 mbar.

5.2. Conductivity properties

Current-voltage behavior of the samples was measured using the previously mentioned method. The measurements were conducted at room temperature, 200 °C and 350 °C. The maximum voltage was lowered to 3 V at higher temperatures due to some samples being damaged at higher voltages. The second loop of the measurement is presented for each sample at each measurement temperature.

Figure 5.6 shows the current-voltage graphs obtained for WO_3 samples. A slight nonlinearity of the data was observed the room temperature measurement of the samples as shown in Figure 5.6 (a), characteristic for semiconductor materials. At higher temperatures however the measurements started to become more linear with little hysteresis present for the 0.08 mbar-sample. The measured current for the 0.08 mbar-sample was much higher than that for the 0.2 mbar-sample.

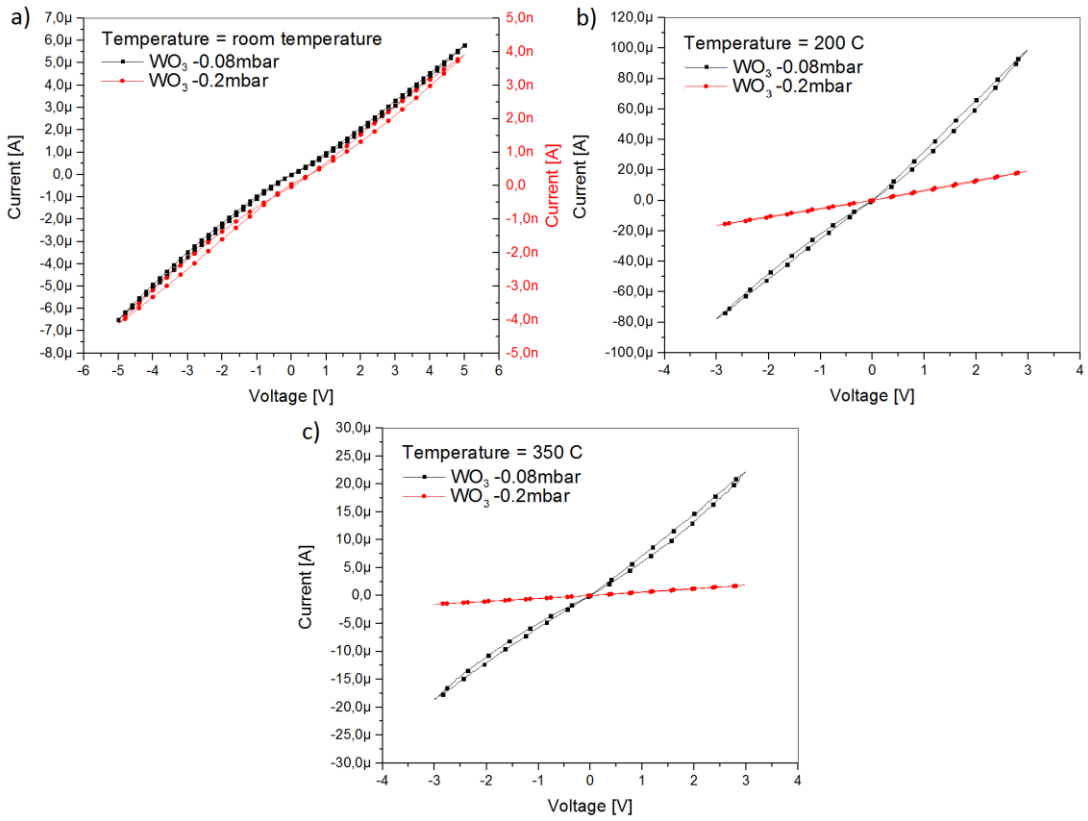

Figure 5.6. Current-voltage graphs for WO_3 samples at (a) room temperature, (b) 200 °C, and (c) 350 °C.

Figure 5.7 illustrates the data obtained from similar measurements done to the SnO_2-ZnO samples. Presence of water vapour, or residual gases from measurements or otherwise, inside the porous structure of the oxide may account for the anomalous behavior of current in the room temperature measurement for SnO_2-ZnO samples. Due to heating from the measurement voltage and the hotplate, the water vapour vaporizes and no longer affects the measurements, as seen in Figures 5.7 (b) and (c). The measurement for SnO_2-ZnO with added platinum was redone by first saturating the measurement chamber with argon before the measurements. A similar anomaly was found in the room temperature measurement in argon atmosphere as well, which was again resolved by heating the sample with the hotplate, or by doing multiple subsequent measurements. This further implies that most likely water vapour adsorbed by the porous structure of the oxide was causing the effect.

From Figure 5.7, it is evident that oxygen partial pressure during PLD played the largest role in determining the current-voltage behavior of the samples. It seemed that platinum particles in the $p(O_2)$ = 0.1 mbar sample only affected room temperature measurements compared to the closest sample of $p(O_2)$ = 0.08 mbar. Although, SEM micrographs obtained from the samples showed that the sample containing platinum had a slightly more porous structure for storing residual gases or water vapour.

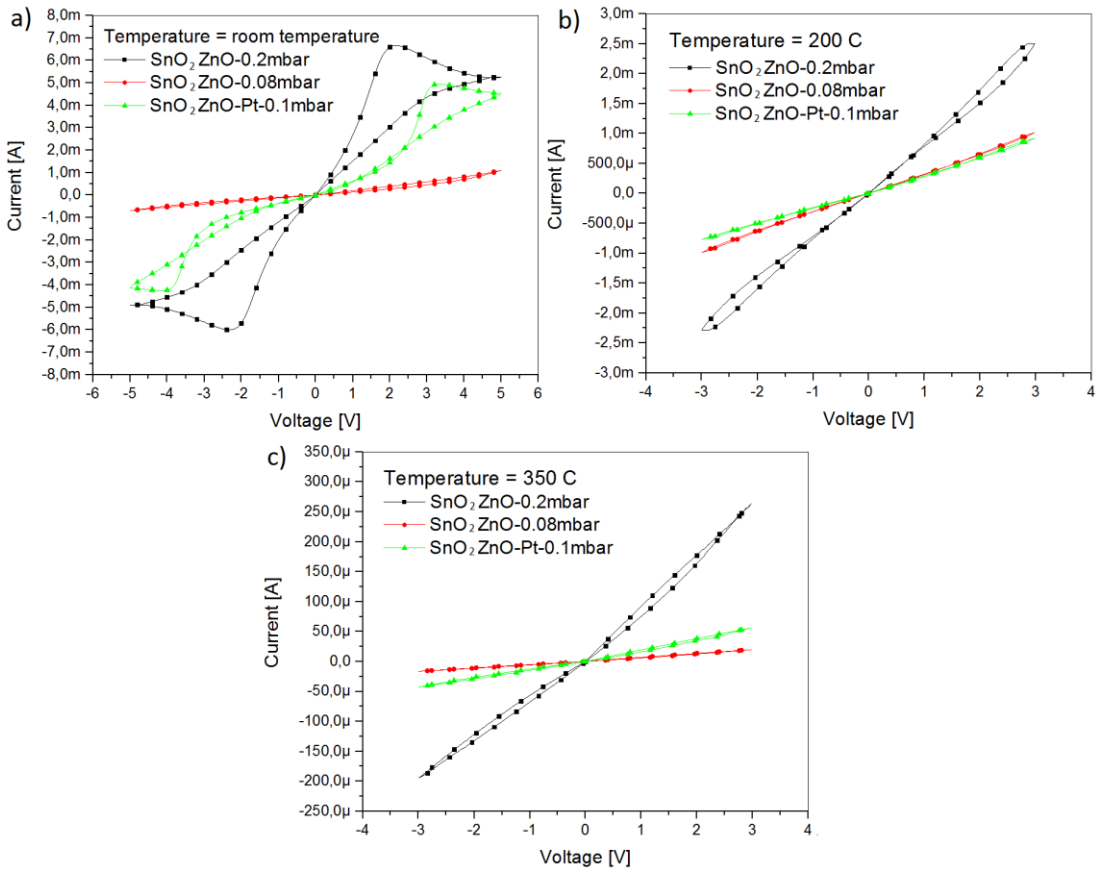

Figure 5.7. Current-voltage graphs for SnO_2-ZnO samples at (a) room temperature, (b) 200 °C, and (c) 350 °C.

As seen in the SEM micrographs of the V_2O_5 samples, the structure of the oxide was quite uniform compared to WO_3 and SnO_2-ZnO. Therefore, the stable nature of the current-voltage graphs for V_2O_5 in Figure 5.8 were to be expected. The results for the current-voltage measurements for the V_2O_5 samples were the most linear of all measured samples. Compared to the room temperature measurement, current increased dramatically in the 200 °C measurement, but the measurements done at 200 °C and 350 °C were almost identical.

The increase in conductivity for WO_3 from room temperature to 200 °C can be explained by donors in the material not being fully ionized at room temperature. However, when temperature was increased to 350 °C, the conductivity of the material dropped closer to that of the room temperature measurement. This is because all donor atoms in the material became ionized causing the resistivity of the material to increase due to more electron scattering caused by increased lattice vibrations. SnO_2-ZnO showed a steadily declining conductivity as temperature increased because all donors were already ionized at room temperature. V_2O_5 presented characteristic behavior as conductivity increased from room temperature to 200 °C, with only minor difference between the 200 °C and 350 °C measurements, i.e., the conductivity saturated.

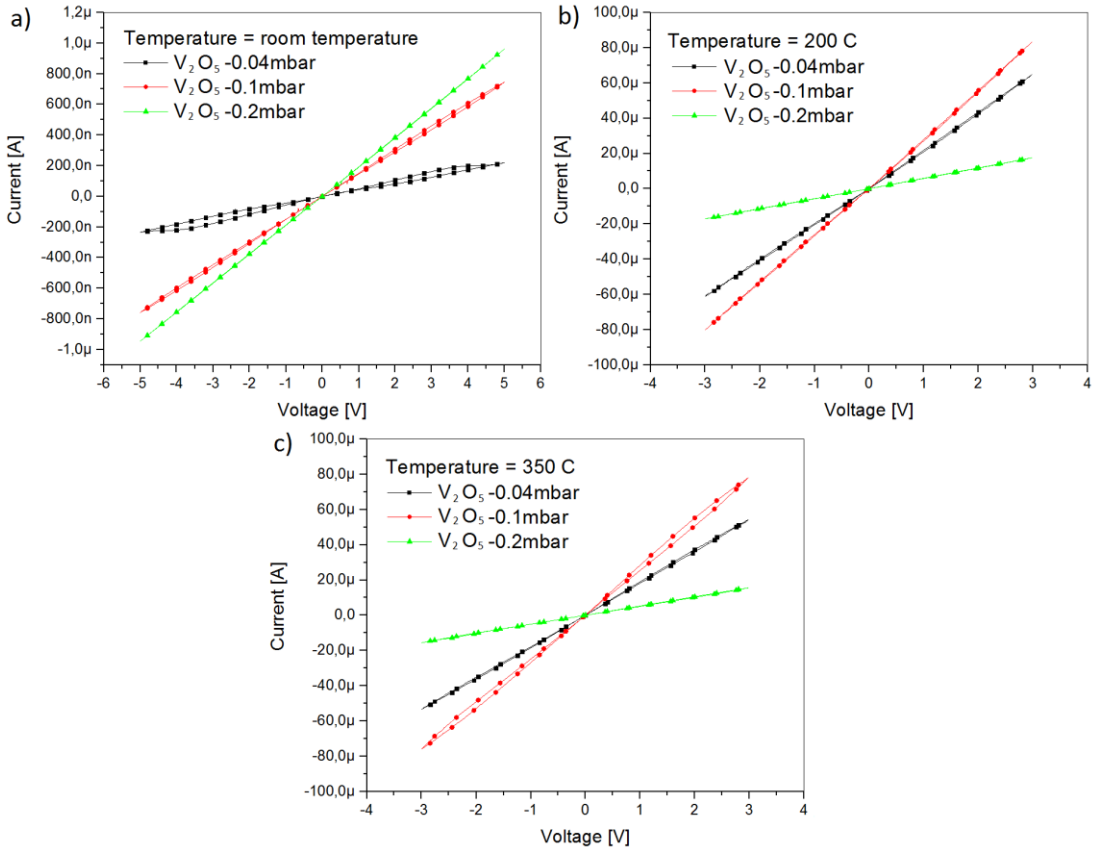

Figure 5.8. Current-voltage graphs for V_2O_5 at (a) room temperature, (b) 200 °C, and (c) 350 °C.

5.3. Gas responses

Gas response measurements were mostly focused on nitrogen oxides and ammonia sensing, with carbon monoxide and hydrogen gas measured as well to determine the cross-sensitivity of the materials towards the gases.

5.3.1. Nitrogen oxides NO_x

Nitrogen oxides gas measurements are presented separately for each material since WO_3 and SnO_2-ZnO samples had an additional NO_x concentration in their measurements. NO_x measurements were done at 200 °C and 350 °C using concentrations of 3, 5, 10, 20, 30, and 50 ppm for both WO_3 and SnO_2-ZnO, and concentrations of 3, 5, 10, 20, and 50 ppm for V_2O_5.

Figure 5.9 shows the NO_x gas measurement data for all WO_3 samples. WO_3 sample prepared in 0.2 mbar oxygen pressure clearly has a more stable, and lower response to NO_x. The 0.2 mbar-sample also has an oxidizing reaction with the gas during the entire measurement.

As for the sample prepared in 0.08 mbar oxygen partial pressure, the response at 200 °C was complex at lower concentrations showing a rapid oxidizing reaction at the beginning of the gas pulse, after which the reaction turned into a reducing one. This was the case for gas concentrations of 2, 5, and 10 ppm, where at 10 ppm the oxidizing

reaction began to dominate after the initial spike. For the gas pulses with 20 ppm of NO_x and above, the reaction became completely oxidizing showing a very large response to the gas.

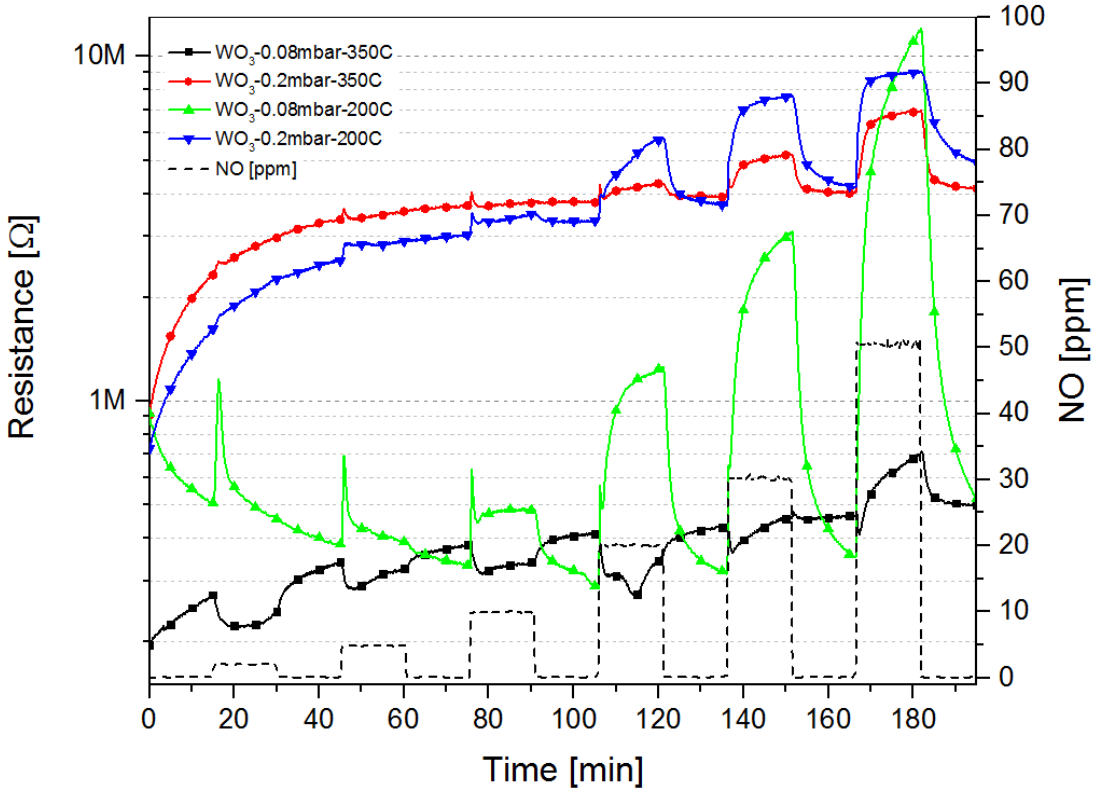

Figure 5.9. NO_x gas responses of WO_3 at measurement temperatures of 200 °C and 350 °C.

At temperature of 350 °C, the 0.08 mbar-sample yet again showed complex behavior in its gas response. At low concentrations the reaction was reducing, but a flipping of the response was observed at concentrations higher than 10 ppm. At the highest measured concentration of 50 ppm, the response flipped entirely to an oxidizing one, and was also well saturated.

WO_3 sample prepared in 0.08 mbar oxygen partial pressure and measured at 200 °C had the largest response to NO_x. However, at measuring temperature of 350 °C, the 0.2 mbar-sample had a superior response compared to the 0.08 mbar-sample. Low concentration measurements of NO_x using WO_3 may present difficulties due to the complex nature of the response.

Equivalent measurements were made for SnO_2-ZnO samples. Figure 5.10 shows the measurement data for the SnO_2-ZnO samples at both measurement temperatures.

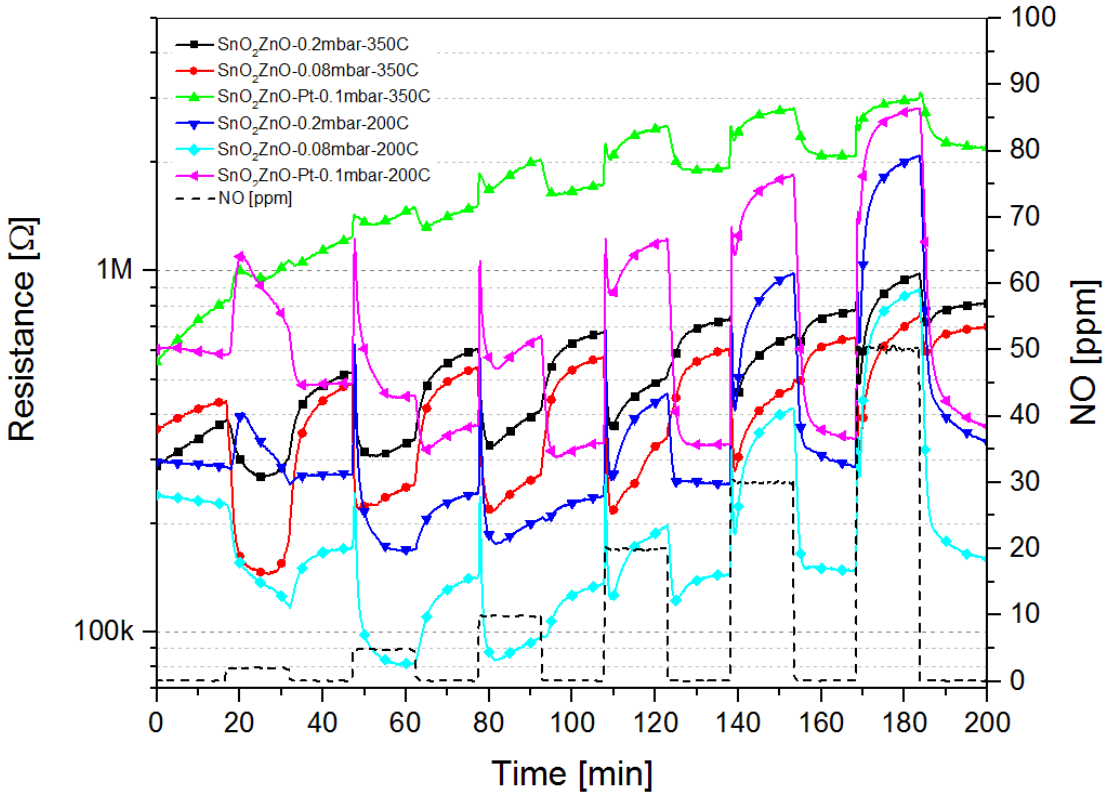

Figure 5.10. NO_x gas responses of SnO_2-ZnO at measurement temperatures of 200 °C and 350 °C.

SnO_2-ZnO samples showed a clearly larger response to NO_x at measuring temperature of 200 °C for all samples. Similarly to WO_3 samples, flipping of the response was present at low concentrations at the 200 °C measurement temperature, and at higher concentrations for the measurement at 350 °C temperature. Responses at 200 °C were fairly similar, but the catalytic effect of added platinum in the 0.1 mbar-sample showed an enhanced reaction compared to other samples. Interestingly, at 350 °C the added platinum turned the entire response to an oxidizing one when compared to the flipping response of the other samples.

Figure 5.11 shows the gas measurement data for V_2O_5 samples. The measurements only differed by number of measured gas concentration, i.e., only 2, 5, 10, 20, and 50 ppm were now measured.

V_2O_5 had a fairly low response to NO_x, overall. One sample, however, had a strong response in all gas concentrations at 200 °C. The 0.04 mbar-sample showed a high reducing response at all concentrations. The sensing ability was, however lost in measurements done at 350 °C. This seemed to be the case for measurements done in other gases, as well. The direction of responses, in general were dependent on measurement temperature. The $p(O_2)$ = 0.04 and 0.2 mbar samples showed an oxidizing reaction to NO_x at 200 °C and a reducing reaction at 350 °C, while the 0.1 mbar-sample showed a reducing reaction at both temperatures. However, the 0.1 mbar-sample had responses that were not in line with the other samples, so conclusions based on its responses are difficult to make.

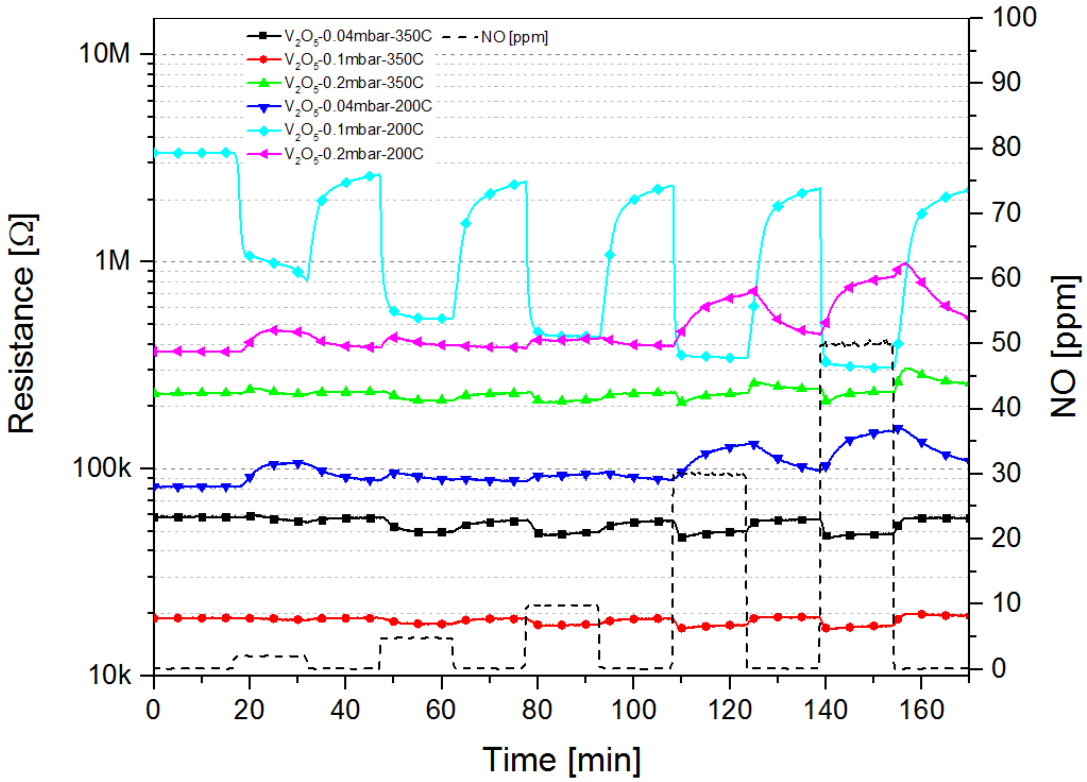

Figure 5.11. NO_x gas responses of V_2O_5 at measurement temperatures of 200 °C and 350 °C.

Figure 5.12 shows the calculated responses $\mathcal{R}$ to NO_x gas for all samples at measurement temperature of 200 °C. Figure 5.12 (a) clearly shows the superior response of WO_3 followed by SnO_2-ZnO. The flipping nature of the NO_x response of both WO_3 and SnO_2-ZnO samples can be seen in the calculated responses shown in Figure 5.12 (b). The flipping behavior of NO_x gas has been previously observed and explained as a complex process of changing interaction with oxygen based on gas concentration and temperature [9].

Calculated response $\mathcal{R}$ to NO_x gas for all samples at measurement temperature of 350 °C can be seen in Figure 5.13. The Figure illustrates the change from a reducing response to an oxidizing response when the concentration of NO_x was increased in the case WO_3 and SnO_2-ZnO samples. The effect of platinum particles in $p(O_2) = 0.1$ mbar of SnO_2-ZnO sample was also clearly seen. The entire response was oxidizing compared to the other SnO_2-ZnO samples, for which the response becomes oxidizing only at the highest concentration. As for the case of V_2O_5, the response was very low and stable for all NO_x concentrations.

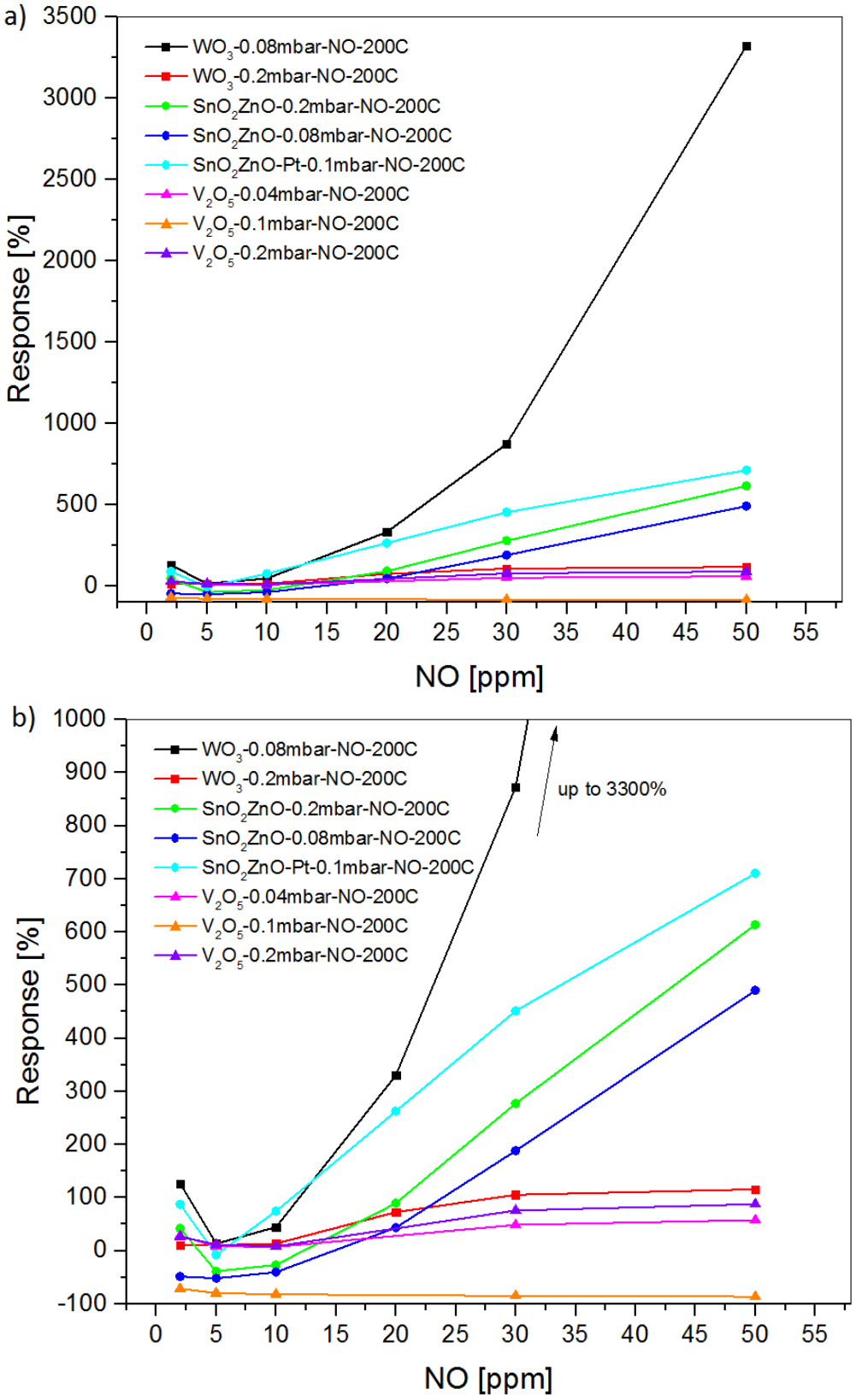

Figure 5.12. NO_x gas responses $\mathcal{R}$ at measurement temperature of 200 °C. (a) Response range up to 3500% and (b) response range up to 1000%.

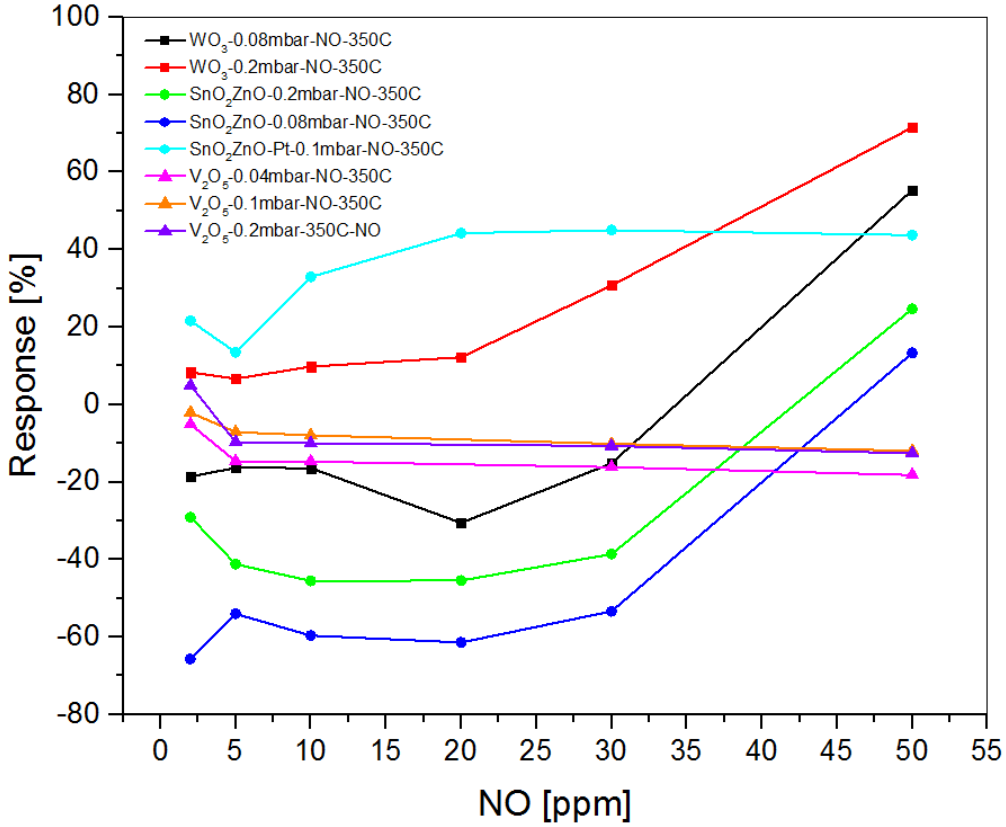

Figure 5.13. NO_x gas responses $\mathcal{R}$ at measurement temperature of 350 °C.

5.3.2. Ammonia NH_3

NH_3 measurement were conducted for the concentrations 3, 5, 10, and 20 ppm. In general, at 200 °C, WO_3 and SnO_2-ZnO samples had the strongest reaction with NH_3. On the other hand, V_2O_5 had a relatively low response with the exception of the 0.1 mbar-sample, which seemed to have the highest response of all the samples. After the NH_3 measurement, however, the baseline resistance of the 0.1 mbar V_2O_5-sample decreased from approximately 6 MΩ to 2 MΩ during the CO measurement. This was probably caused by poisoning of the material by the NH_3. After the NH_3 measurement, the baseline resistance never recovered to the original state when CO and H_2 measurements were done. Figure 5.14 shows the measured responses $\mathcal{R}$ of all materials for NH_3 at measurement temperature of 200 °C. The 0.1 mbar-V_2O_5 response was clearly visible as having the highest response, and the decline of the baseline resistance was also evident.

Figure 5.15 shows the calculated NH_3 gas responses for the measurements done at 200 °C. From the graph, it was evident that all materials had a reducing response to ammonia. V_2O_5 prepared in $p(O_2)$ = 0.1 mbar clearly had the highest response. The other samples had similar responses with different magnitudes. Interestingly, the SnO_2-ZnO sample with added platinum only showed enhanced response at lower concentrations compared to the closest match of 0.08 mbar SnO_2-ZnO sample.

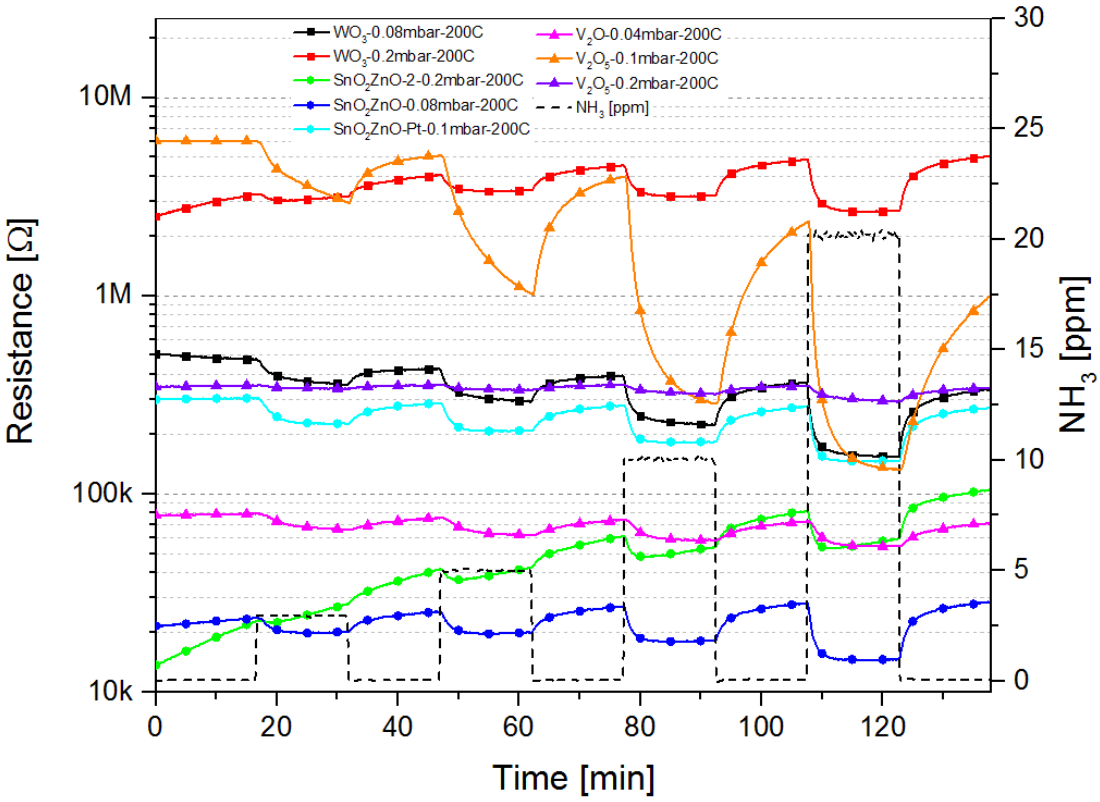

Figure 5.14. NH_3 gas responses $\mathcal{R}$ of all materials at measurement temperature of 200 °C.

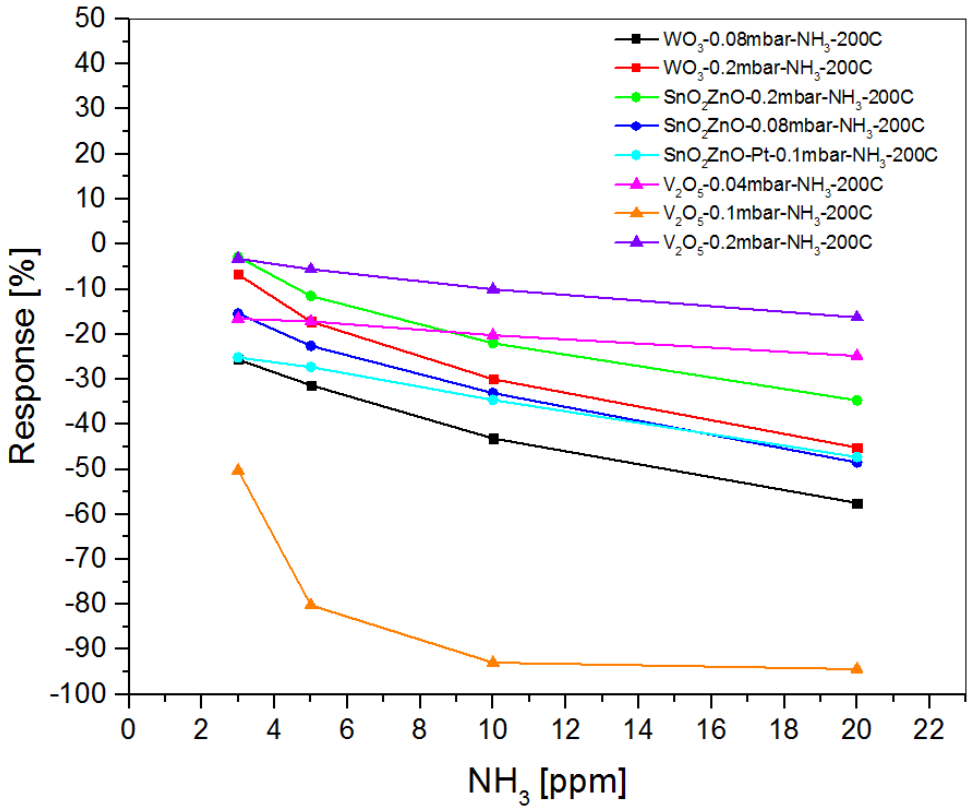

Figure 5.15. NH_3 gas response $\mathcal{R}$ of all materials at measurement temperature of 200 °C.

Measurements done at 350 °C showed that the responses were becoming more similar across the materials except for the 0.08 mbar WO_3 and 0.1 mbar SnO_2-ZnO with platinum particles, which seemed to retain their responsiveness. Figure 5.16 illustrates the NH_3 gas responses of all samples measured at 350 °C. SnO_2-ZnO samples without added platinum showed a slight decrease in response compared to a small increase in response for V_2O_5 samples. The 0.1 mbar V_2O_5-sample response decreased dramatically compared to the measurements done at 200 °C. The figure also shows that the baseline resistance of the 0.1 mbar V_2O_5-sample had drastically deteriorated to a few tens of kiloohms when the baseline at the start of the measurements at 200 °C was at several megaohms.

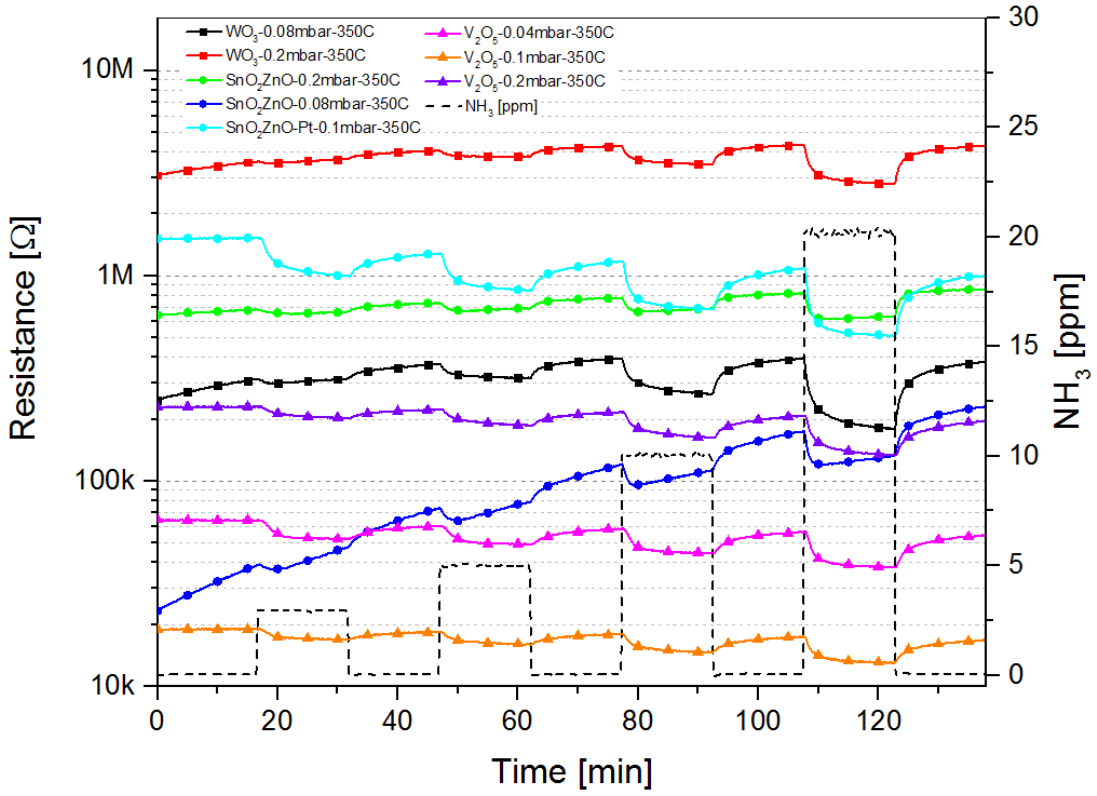

Figure 5.16. NH_3 gas responses of all materials at measurement temperature of 350 °C.

Figure 5.17 shows the calculated NH_3 gas responses $\mathcal{R}$ for all samples measured at 350 °C. Similarly to measurements done at 200 °C, all responses were reductive. In the case of ammonia sensing, platinum particles in the 0.1 mbar SnO_2-ZnO-sample seemed to make the sensors almost temperature independent with only a slight overall increase in response compared to the measurement at 200 °C.

Generally, the 0.08 mbar WO_3 and 0.1 mbar SnO_2-ZnO-sample with added platinum had the highest and most stable responses. The case of the 0.1 mbar V_2O_5-sample presented some problems in evaluating its performance.

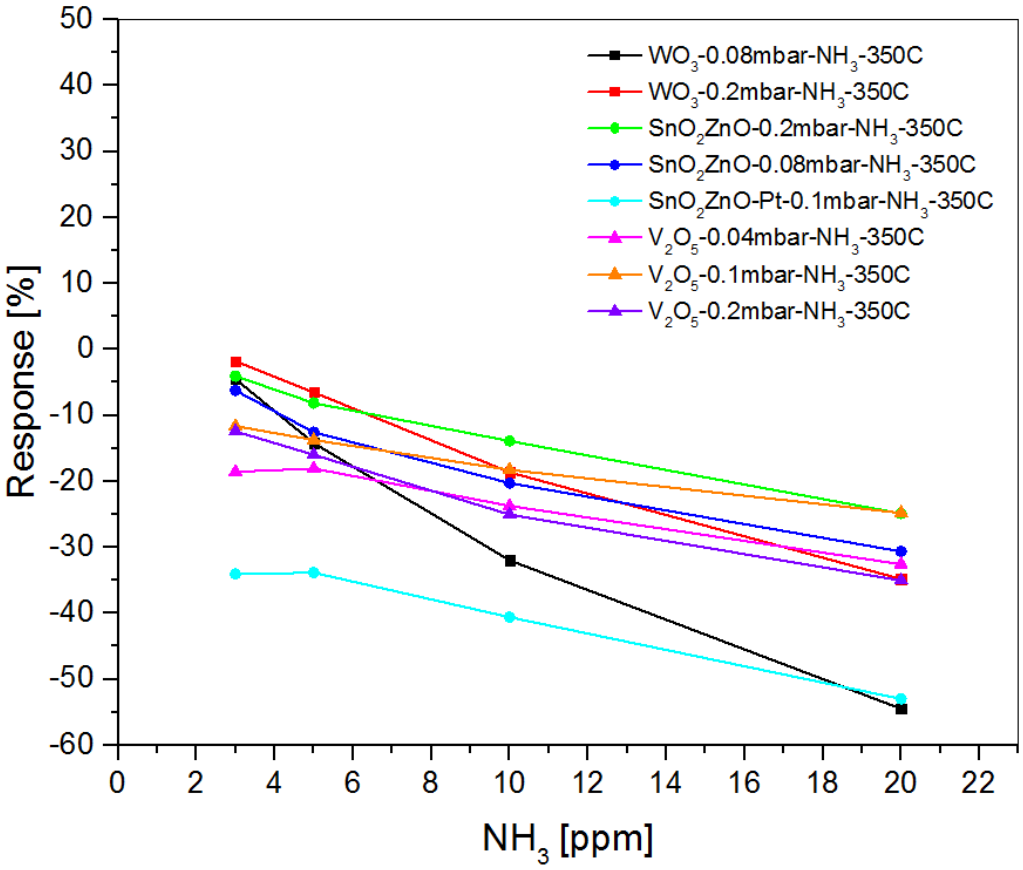

Figure 5.17. NH_3 gas responses $\mathcal{R}$ of all materials at measurement temperature of 350 °C.

5.3.3. Carbon monoxide CO

The sensors used in this study were mainly designed on sensing NO_x and NH_3, so CO measurements were done mostly to check cross-sensitivity of the sensors. The measurements were conducted on all samples in both measurement temperatures. Several CO concentration levels, including 20, 40, 100, and 200 ppm, were measured. Figure 5.18 shows the data for the CO measurement done at 200 °C. The graph shows that SnO_2-ZnO samples had the highest response to carbon monoxide compared to other materials with the exception of the 0.1 mbar V_2O_5-sample. WO_3 and V_2O_5 samples had actually a very low response, which can be seen as an advantage in some applications due to constant presence of carbon oxides in the atmosphere.

All the measurements showed a gradual downward drift of the baseline of sensor resistance. This may have simply been due to insufficient time between CO pulses in the measurement. However, for the 0.1 mbar V_2O_5-sample the baseline was again rapidly decreased from 2 MΩ to 1 MΩ during the measurement. The baseline never recovered from the decrease. Every material also showed a reducing response as was to be expected from the *n*-type materials used in the measurements.

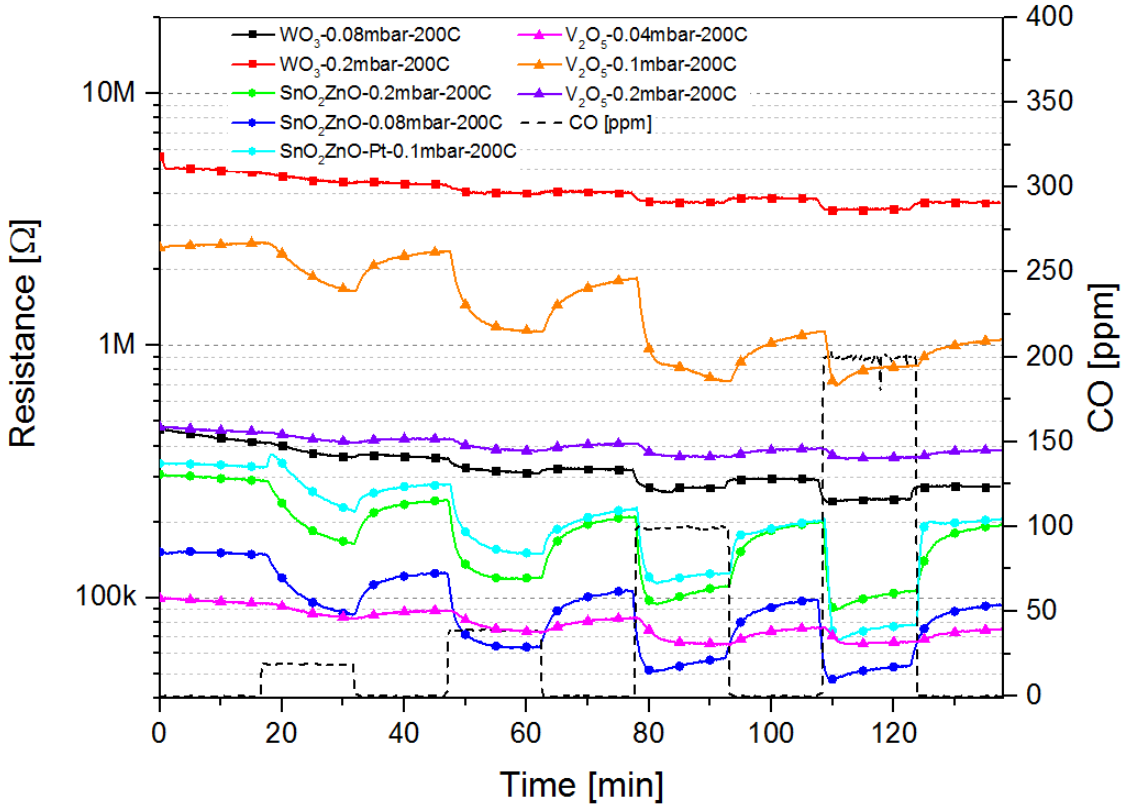

Figure 5.18. CO gas responses of all materials at measurement temperature of 200 °C.

The calculated CO gas responses $\mathcal{R}$ at measurement temperature of 200 °C can be seen in Figure 5.19. The graph clearly shows the higher response of SnO_2-ZnO compared to other materials with the exception of one V_2O_5 sample. Interestingly, the magnitude of the response to CO was fairly similar regardless of concentration for all materials. The stable nature of the response may present problems for determining the concentration of CO through the sensor resistance change. However, a predictable response to CO at many concentration levels may prove beneficial in measuring other gases, to which the sensor may be more responsive, as is the case for both WO_3 and V_2O_5.

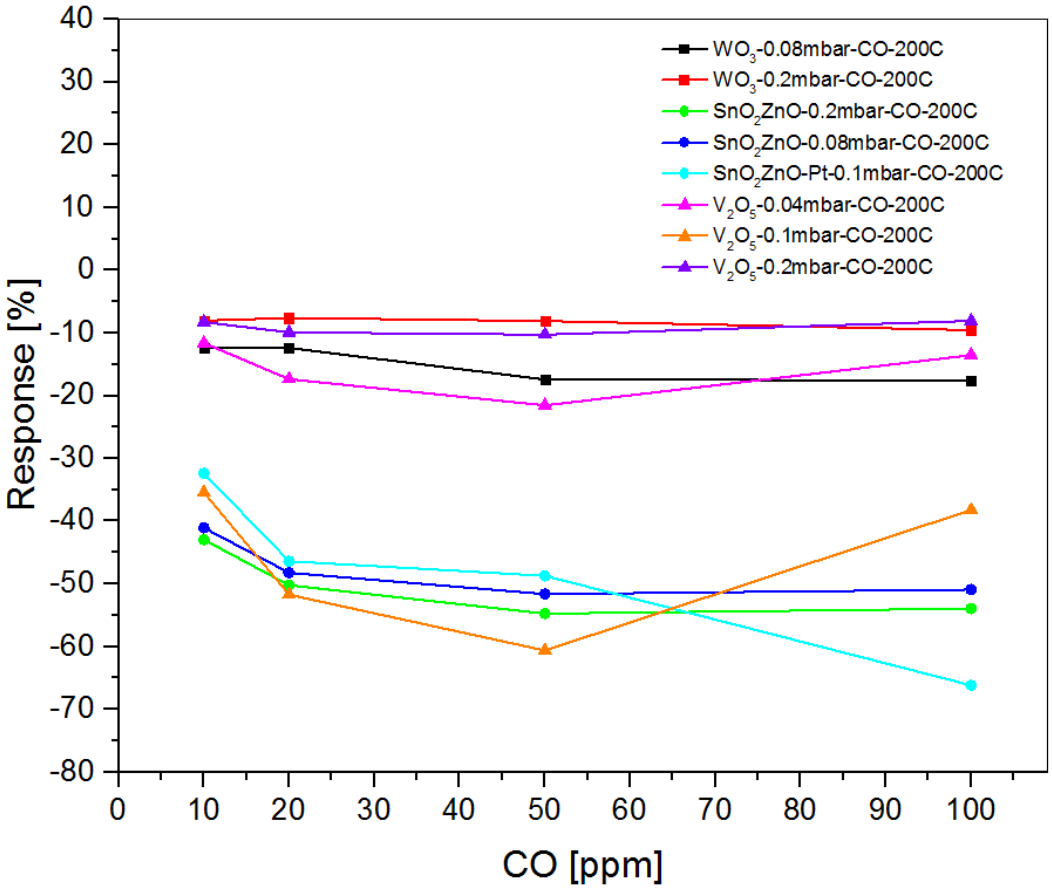

Figure 5.19. CO gas responses $\mathcal{R}$ of all materials at measurement temperature of 200 °C.

Figure 5.20 shows the data for measurement done at 350 °C. Similar conclusions compared to the 200 °C case can be made; the response was in all cases reductive and SnO_2-ZnO samples had the largest response, as can be seen in Figure 5.21. Similarly to measurement done at 200 °C, WO_3 and V_2O_5 both had very stable responses regardless of gas concentration. As before, V_2O_5 sample prepared in $p(O_2) = 0.1$ mbar showed a distinct drop in response when measurements were done at 350 °C.

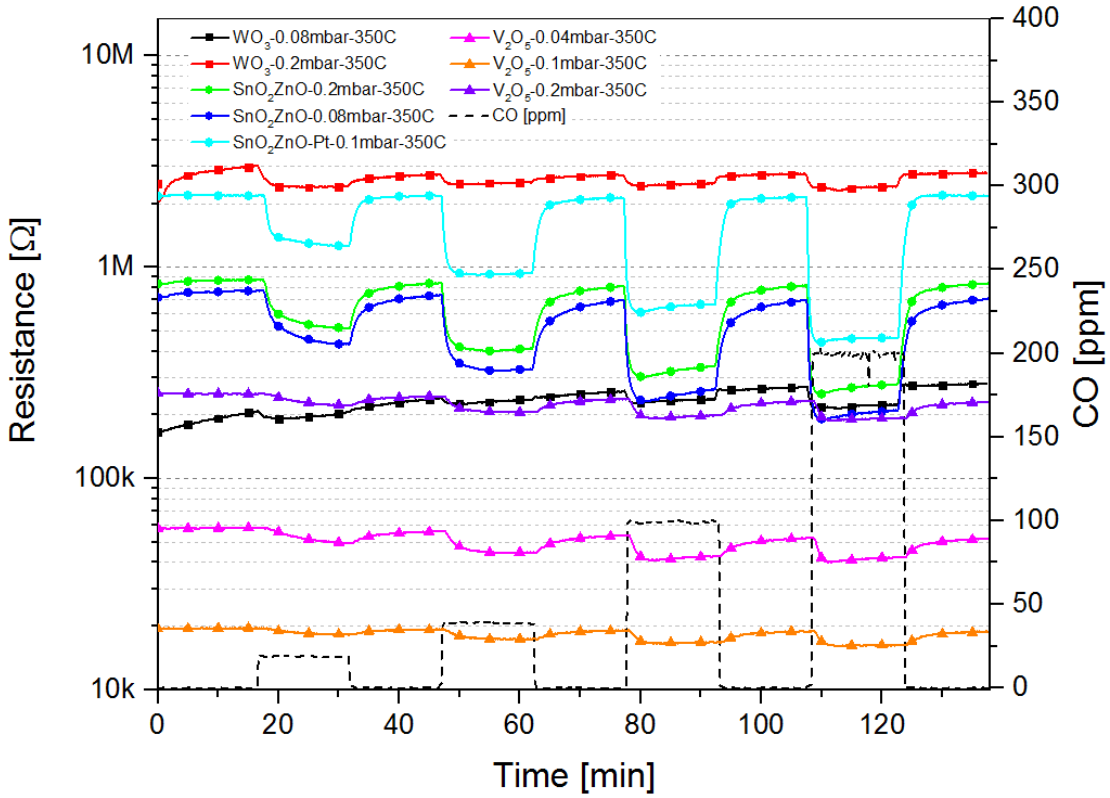

Figure 5.20. CO gas responses of all materials at measurement temperature of 350 °C.

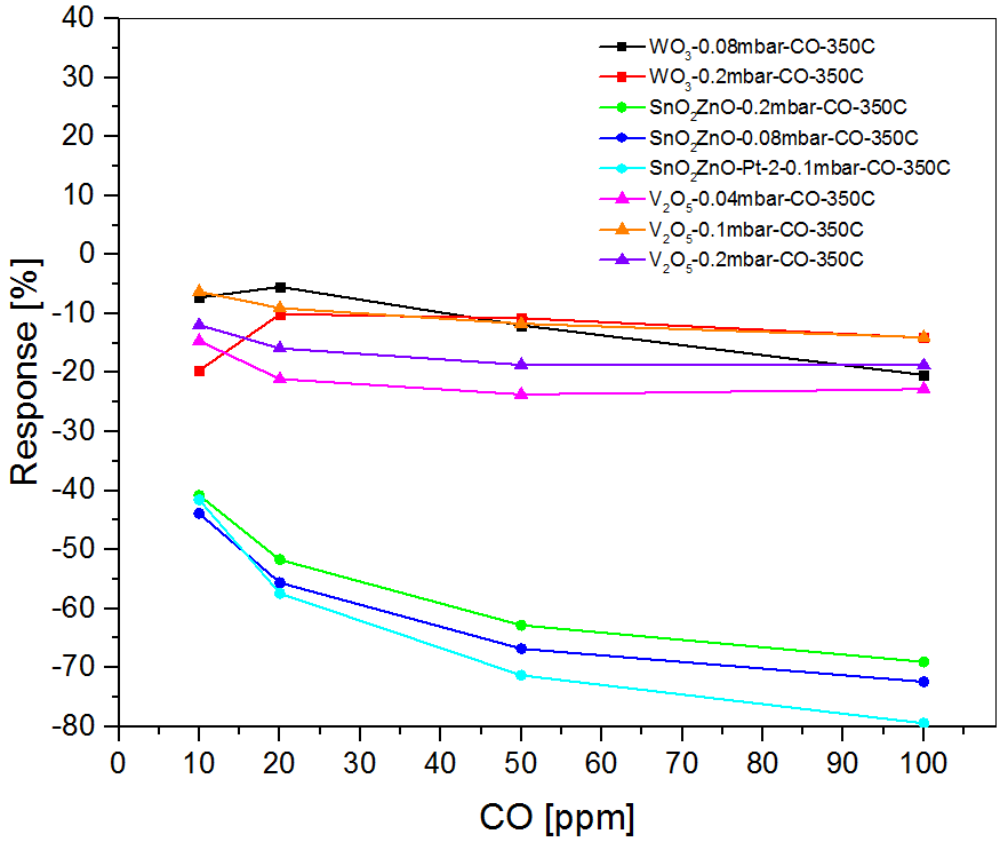

Figure 5.21. CO gas responses $\mathcal{R}$ of all materials at measurement temperature of 350 °C.

5.3.4. Hydrogen H_2

As with CO, H_2 gas measurements were mostly done to evaluate cross-sensitivity characteristics of the sensors. Therefore, for the sensors in this study, having a low response to hydrogen can be seen as an advantage. Hydrogen concentrations that were measured included 70, 90, 140, and 200 ppm. The concentrations were high due to a combination of the high concentration of the H_2 source and having to keep the overall gas flow in the chamber as low as possible to avoid unnecessary cooling of the sensor.

Figure 5.22 shows the data for H_2 gas measurement done at 200 °C. In general, WO_3 and V_2O_5 samples showed a very low response to H_2, with the exception of the 0.1 mbar V_2O_5-sample. SnO_2-ZnO samples on the other hand showed a complex response where the 0.2 mbar-sample and the 0.1 mbar-sample with platinum had a very similar response, but the enhancing effect of the platinum particles was clearly visible. However, the 0.08 mbar SnO_2-ZnO-sample showed a reverse reaction compared to the other samples; the sample had a complex flipping reaction at low concentrations and a reducing reaction at higher concentrations. The 0.1 mbar and 0.2 mbar samples had an oxidizing reaction at low concentrations and at higher concentrations showed a minor reducing reaction.

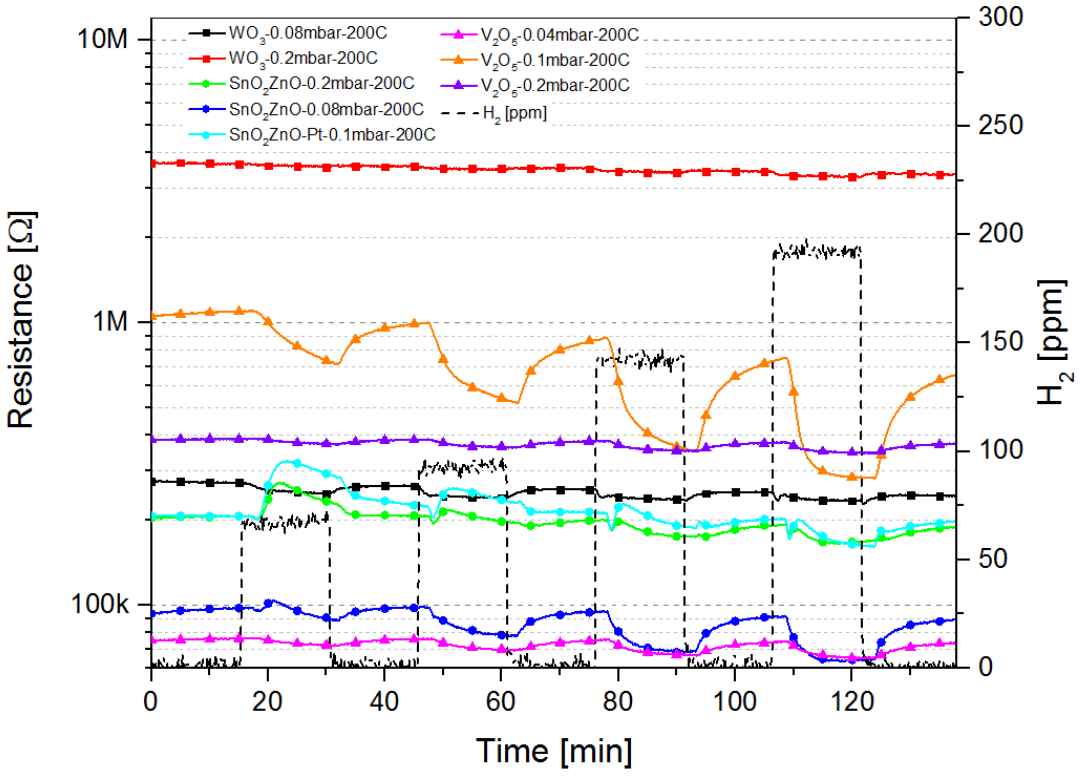

Figure 5.22. H_2 gas responses of all materials at measurement temperature of 200 °C.

The calculated responses $\mathcal{R}$ for hydrogen at 200 °C can be seen in Figure 5.23. The flipping nature of the response for SnO_2-ZnO samples was very clear as was the low and stable response of WO_3 and V_2O_5 samples, with the exception of the 0.1 mbar V_2O_5-sample. The enhancing effect of platinum particles in the 0.1 mbar SnO_2-ZnO samples was also visible.

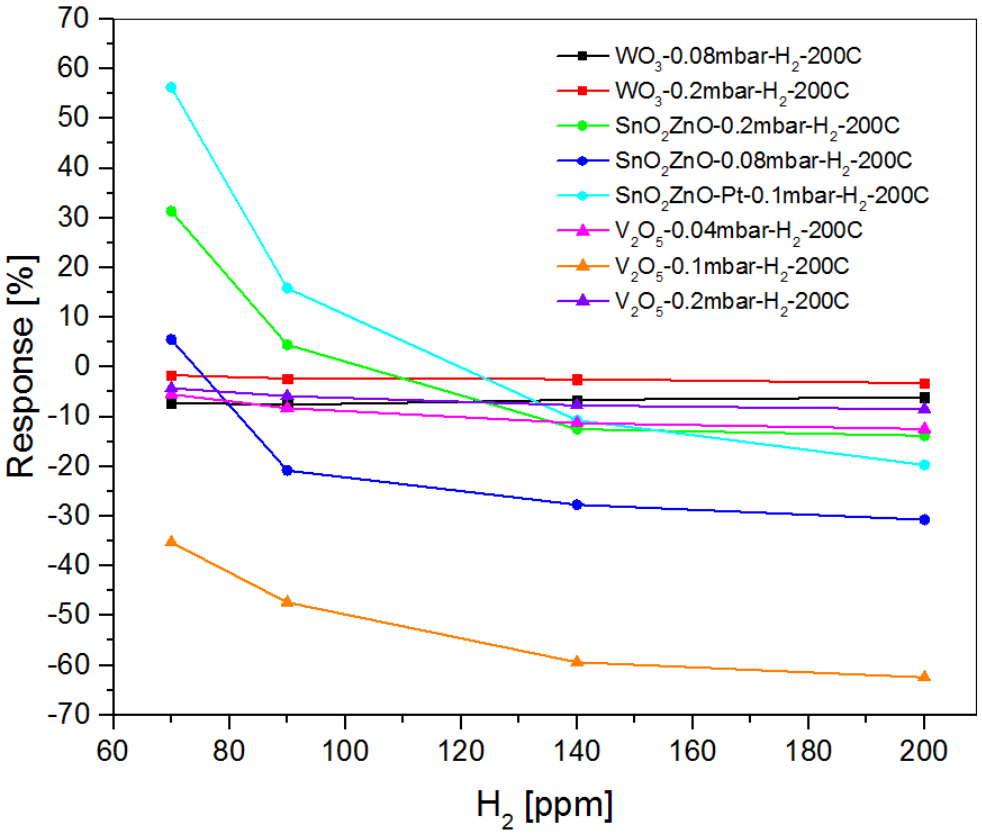

Figure 5.23. H_2 gas responses $\mathcal{R}$ for all materials at the measurement temperature of 200 °C.

At the higher measurement temperature the gas responses were much more consistent, as shown in Figure 5.24. The response of all materials were reducing across all concentrations. WO_3 and V_2O_5 samples had a fairly low response in all cases. SnO_2-ZnO samples, as previously, showed a much higher response to the presence of H_2, however the concentration of the gas didn't seem to have much of an impact compared to the measurement done at 200 °C. The enhancing effect of the platinum particles in the 0.1 mbar sample was again clearly observable.

Figure 5.25 shows the calculated responses $\mathcal{R}$ for H_2 of all materials at 350 °C. The responses were clearly almost independent of H_2 concentration with only minor change in response as H_2 concentration increases. Generally, WO_3 and V_2O_5 were the most non-responsive towards hydrogen while SnO_2-ZnO showed a quite high response for low concentrations at 200 °C and all concentrations at 350 °C.

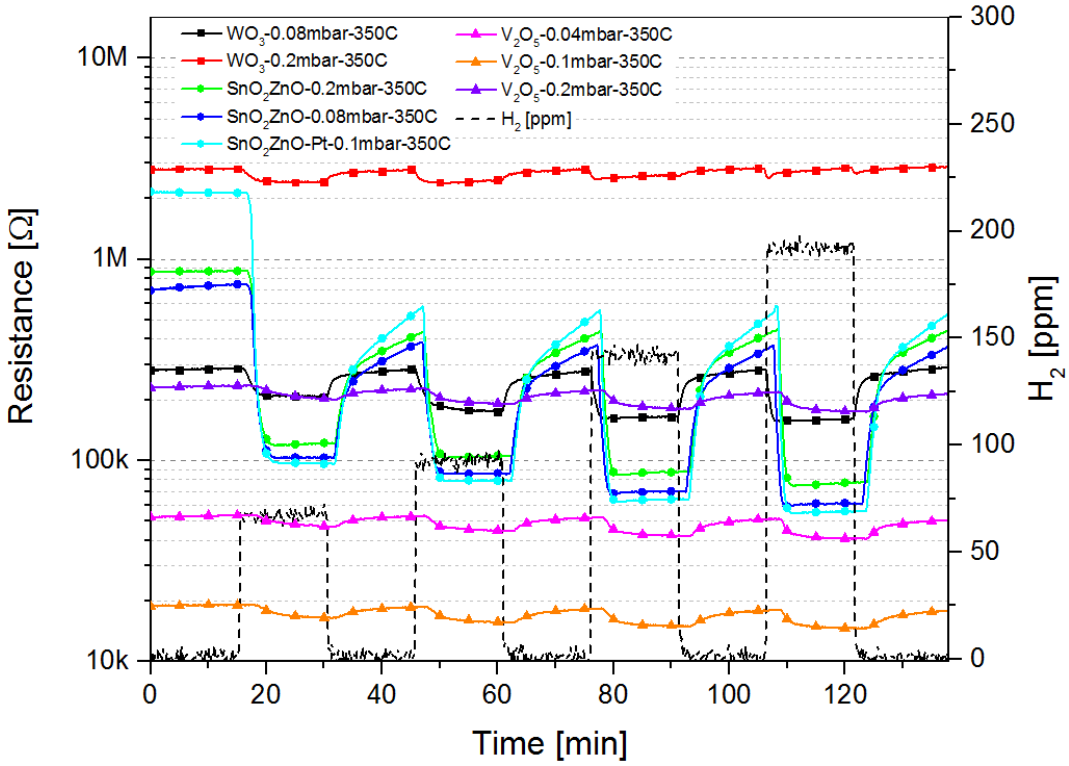

Figure 5.24. H_2 gas responses of all materials at measurement temperature of 350 °C.

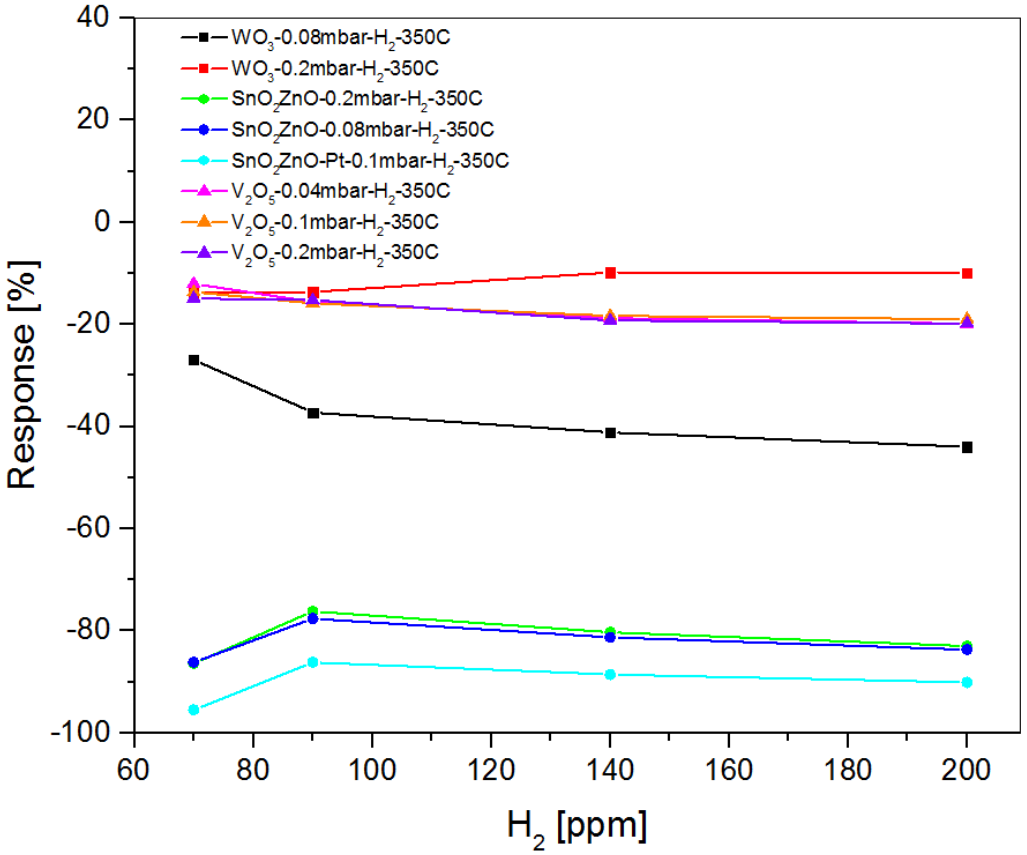

Figure 5.25. H_2 gas response $\mathcal{R}$ of all materials at measurement temperature of 350 °C.

5.3.5. Selectivity

Gas response data was analyzed against any selective behavior towards studied gases. Overall, SnO_2-ZnO samples were most responsive towards all types of gases with NO_x causing the largest response, while WO_3 and V_2O_5 samples showed selective behavior towards NO and NH_3. Figure 5.26 displays the selectivity of WO_3 at measurement temperature of 200 °C. Both samples showed selectivity towards NO_x while CO, and H_2 responses remained low. NH_3 response, however is noticeable. Similar selectivity was observed in measurements done at 350 °C, but the responses were considerably smaller, especially those for NO_x.

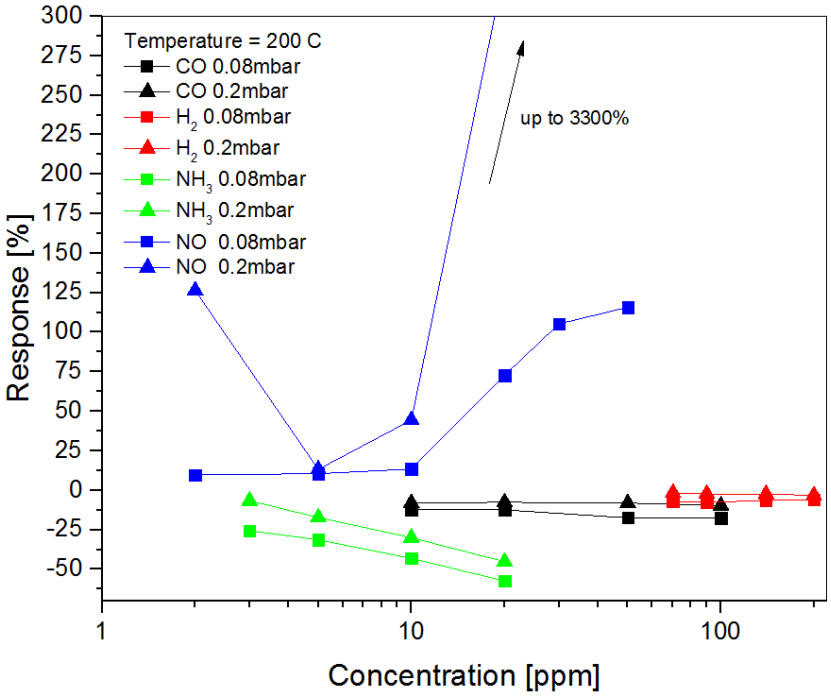

Figure 5.26. WO_3 gas responses $\mathcal{R}$ of both samples at 200 °C.

SnO_2 is, in general, considered highly reactive to almost any type of gaseous stimulant. This behavior was observed for the SnO_2-ZnO samples in measurements, but tendency to have the largest response to NO_x was clearly visible across all of the SnO_2-ZnO samples. Figure 5.27 shows the selective nature of SnO_2-ZnO gas responses. All SnO_2-ZnO samples exhibited somewhat similar behavior towards all gases with the sample including platinum particles, having an enhanced reaction compared to the other samples.

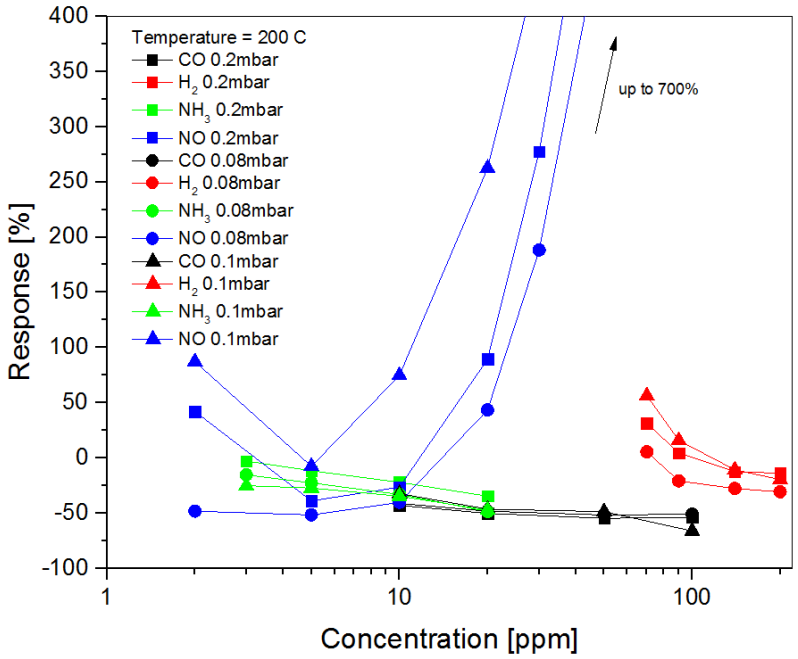

Figure 5.27. SnO_2-ZnO gas responses $\mathcal{R}$ for all samples at 200 °C.

V_2O_5 sample prepared in 0.2 mbar oxygen partial pressure displayed interesting selective behavior; at 200 °C the sample was most responsive to NO_x, while at 350 °C the sample reacted the strongest to NH_3. Figure 5.28 illustrates this behavior. At 200 °C, the sample showed a maximum oxidizing NO_x response of almost 90% while the reducing ammonia response remains below 15%. When the measurement temperature was increased to 350 °C, the NO_x response became more complex, having both oxidizing and reducing reactions, and considerably smaller in magnitude, remaining within 10%. At the same time, the reducing NH_3 response of the sample increases up to 35%.

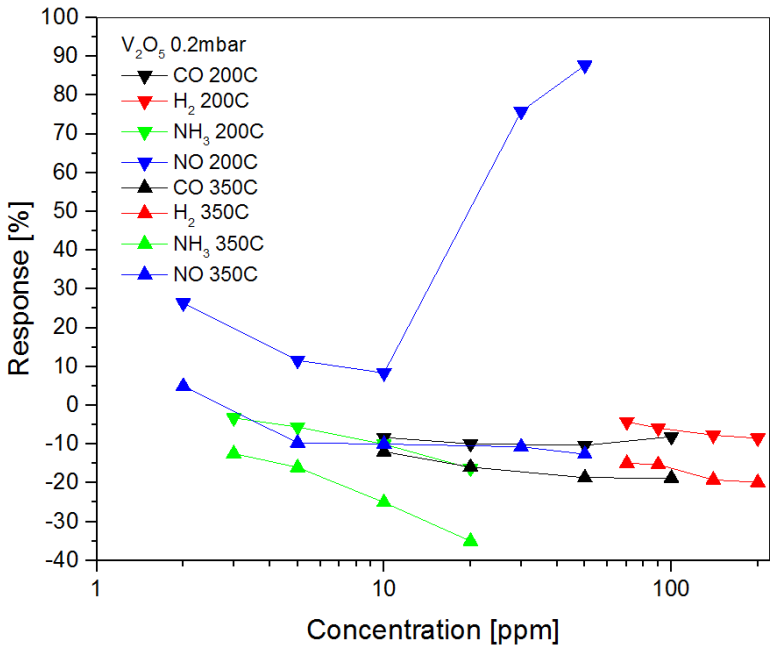

Figure 5.28. V_2O_5 gas responses $\mathcal{R}$ of all gases and both measurement temperatures for the sample prepared in 0.2 mbar oxygen partial pressure.

5.4. Selective catalytic reduction (SCR) properties

Selective catalytic reduction (SCR) is a process which involves the use of reductant, typically ammonia or urea, to convert nitrogen oxides into diatomic nitrogen and water. The process is applied in, for example, industrial boilers and diesel engines.

A SCR environment experiment was conducted on a V_2O_5-sample prepared in 0.2 mbar oxygen partial pressure in PLD. The result of the measurement can be seen in Figure 5.29. The SCR process experiment was conducted as follows: up until point 1 (see Figure 5.29) only synthetic air was flowing in the measurement chamber, while the microheater in the sensor was kept at a temperature of 300 °C. Point 1 marks the moment when CO with 100 ppm concentration was introduced into the gas flow. CO caused a fast decline of resistance and began to saturate after the response flipped. Then 20 ppm of NO_x entered the gas flow at point 2 and caused rapid lowering of resistance at first, but then flipped back towards saturation. However, as 20 ppm of NH_3 joined the gas flow at point 3, a large reductive response was observed in the data. This indicated that V_2O_5 had a clear selective behavior towards NH_3.

The experiment continued as NO_x flow was halted at point 4. A small increase in resistance was found to occur after NO_x flow was no longer present. Next, at point 5, the NH_3 flow was also halted and a rapid increase in resistance was observed again. The response was not able to fully saturate as the next NH_3 pulse was started at point 6. Again, a rapid decrease of resistance was observed in the data. At point 7, NO_x was yet again introduced into the gas flow and a rather small response was observed. Resistance saturated fairly fast after NO_x entered the gas flow. At point 8, NH_3 flow was halted and a similar increase in resistance was observed as at point 5. Finally, NO_x flow was also halted at point 9, where the resistance saturates close to the value observed at point 2, when NO_x was first introduced into the gas flow, i.e. resistance recovered close to its initial value.

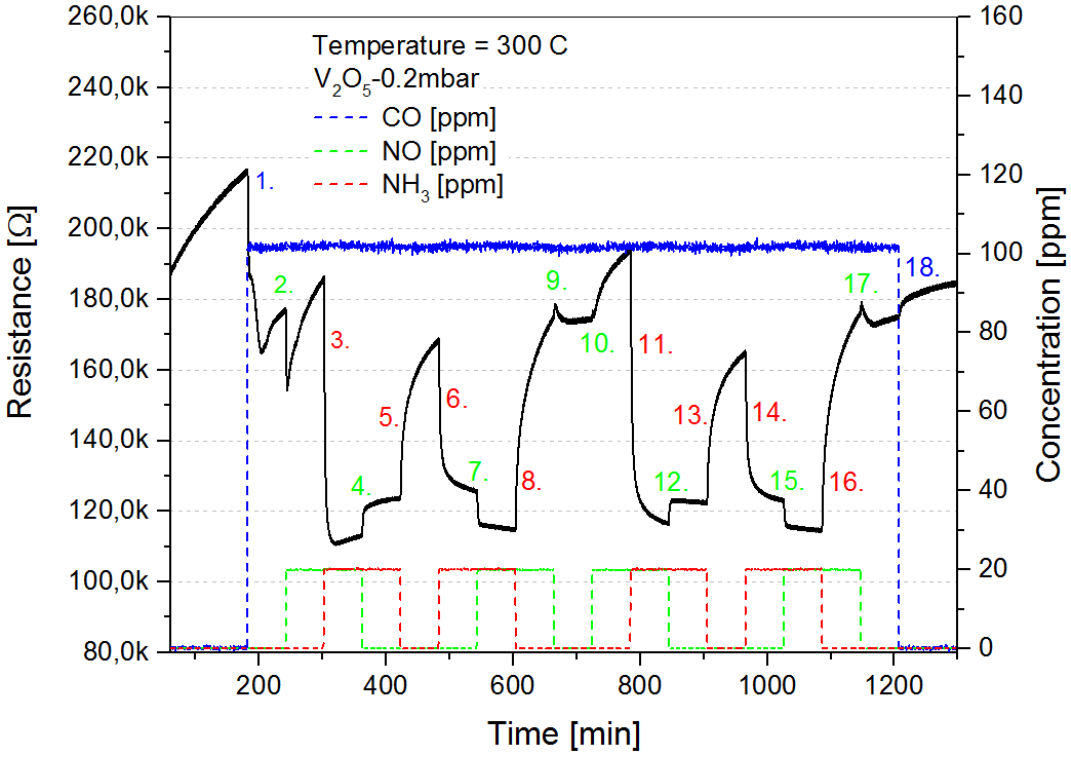

Figure 5.29. SCR environment experiment conducted on a V_2O_5 sample.

The process from point 2 to point 9 was repeated from point 10 to point 17, and at point 18 only synthetic air flow remained as the resistance began to slowly rise. A very similar graph was obtained from the second round of the process, which showed the fairly stable nature of V_2O_5 as a gas sensor. The results indicated the feasibility for controlling process parameters in a selective catalytic reduction process.

The relatively small NO_x response during the process may be explained by the fact that CO present in the gas flow had already occupied sites where nitrogen oxides would normally adsorb during the interaction. NH_3, on the other hand, caused a different reaction with V_2O_5, and was therefore seen to have a large effect on the sensor resistance even in the presence of CO and NO_x. The large NH_3 response may be credited to the layered microstructure of the V_2O_5, in which ammonia starts to occupy spaces between layers unlike CO and NO_x, whose reaction is based on binding with preadsorbed oxygen atoms and, in the case of dioxides, serving as receptors for electrons on the oxide surface.

6. CONCLUSIONS

Resistive metal-oxide gas sensors based on SGX Sensortech S.A. MEMS microhotplate platforms were prepared using PLD as the deposition method. Deposited materials included WO_3, SnO_2-ZnO, and V_2O_5 prepared in different oxygen partial pressures during deposition. Surface and microstructure of the samples were studied with X-ray diffraction, Raman spectroscopy, AFM, and SEM. Current-voltage behavior was measured and analyzed. Samples were subjected to different concentrations of various gases, including NO_x, NH_3, CO, and H_2, at measurement temperatures of 200 °C and 350 °C, and the responses were analyzed.

The structures found by different characterization methods were compared to measured gas responses. Oxygen partial pressure ($p(O_2)$) during PLD had a clear impact on the microstructure of the oxide film. Higher $p(O_2)$ resulted in larger agglomerates of particles, which in general, led to lower gas sensitivity due to factors such as grain size and surface area-to-volume ratio.

Gas measurements were conducted in NO_x, NH_3, CO and H_2 gas. The measurements show high responses for NO_x for WO_3 and SnO_2-ZnO samples, as expected. Also, flipping of the response from reductive for low concentration to oxidizing for high concentration was observed for WO_3 and SnO_2-ZnO, while V_2O_5 showed a mostly stable response. One of the V_2O_5 samples showed extremely high responses to all measured gases in low temperature measurements, but lost its gas sensing properties at the higher temperature measurement. Decline of the resistance was observed throughout the measurement process at the lower temperature, with largest drop in baseline resistance observed in the NH_3 measurement, suggesting that some kind of poisoning of the material occurred. Overall, WO_3 showed selectivity towards NO_x, while SnO_2-ZnO was highly responsive to all gases depending on measurement conditions with NO_x generating the highest response. V_2O_5 showed low responses to CO and H_2 gas, but high sensitivity and selectivity toward both NO_x and NH_3 depending on measurement temperature.

An experiment of a selective catalytic reduction environment was conducted for a selected V_2O_5-sample. The sample had distinct reactions to all the gases including CO, NO_x, and NH_3 used in the measurement, with the highest response to NH_3. This experiment was promising for the practical applications of V_2O_5 nanoparticle based gas sensors.

7. REFERENCES

[1] Taguchi N. (1962) Published patent application in Japan, S37-47677, Oct.

[2] Seiyama T., Kato A., Fujiishi K. & Nagatani M. (1962) A new detector for gaseous components using semiconductive thin films. *Analytical Chemistry, 34*(11), 1502-1503.

[3] Yamazoe N. & Shimanoe K. (2013) Fundamentals of semiconductor gas sensors. *Semiconductor Gas Sensors*, 1.

[4] Yamazoe N., Sakai G. & Shimanoe K. (2003) Oxide semiconductor gas sensors. *Catalysis Surveys from Asia*, *7*(1), 63-75.

[5] Yamazoe N. & Shimanoe K. (2013) Fundamentals of semiconductor gas sensors. *Semiconductor Gas Sensors*, 1.

[6] Brattain W.H. & Bardeen J. (1953) *Bell System Techical Journal*, *32*(1), 1-41.

[7] Barsan N, & Weimar U. (2001) Conduction model of metal oxide gas sensors. *Journal of Electroceramics*, *7*(3), 143-167.

[8] Shankar P. & Rayabban J.B.B. (2015) Gas sensing mechanism of metal oxides: The role of ambient atmosphere, type of semiconductor and gases - A review. *ScienceJet* 4(126), 1-18.

[9] Ruhland B., Becker T. & Müller G. (1998) Gas-kinetic interactions of nitrous oxides with SnO_2 surfaces. *Sensors and Actuators B: Chemical*, *50*(1), 85-94.

[10] Wurzinger O. & Reinhardt G. (2004) CO-sensing properties of doped SnO_2 sensors in H_2-rich gases. *Sensors and Actuators B: Chemical*, *103*(1), 104-110.

[11] Takao Y., Miyazaki K., Shimizu Y. & Egashira M. (1994) High Ammonia Sensitive Semiconductor Gas Sensors with Double-Layer Structure and Interface Electrodes. *Journal of the Electrochemical Society*, *141*(4), 1028-1034.

[12] Jimenez I., Centeno M.A., Scotti R., Morazzoni F., Cornet A., & Morante J.R. (2003) NH_3 Interaction with Catalytically Modified Nano-WO_3 Powders for Gas Sensing Applications. *Journal of the Electrochemical Society*, *150*(4), H72-H80.

[13] Yamazoe N. & Shimanoe K. (2009) Receptor function and response of semiconductor gas sensor. *Journal of Sensors*, 21 pages.

[14] Batzill M. & Diebold U. (2005) The surface and materials science of SnO_2-ZnO. *Progress in surface science*, *79*(2), 47-154.

[15] Lantto, V. (1992) Semiconductor gas sensors based on SnO_2 thick films. In *Gas Sensors* (pp. 117-167). Springer Netherlands.

[16] Yamazoe N. (1991) New approaches for improving semiconductor gas sensors. *Sensors and Actuators B: Chemical*, *5*(1), 7-19.

[17] Xu C., Tamaki J., Miura N. & Yamazoe N. (1991) Grain size effects on gas sensitivity of porous SnO_2-based elements. *Sensors and Actuators B: Chemical*, *3*(2), 147-155.

[18] Rothschild, A., Komem, Y. (2004) The effect of grain size on the sensitivity of nanocrystalline metal-oxide gas sensors. *Journal of Applied Physics, 95*(11), 6374-6380.

[19] Zaretskiy N.P., Menshikov L.I. & Vasiliev A.A. (2012) On the origin of sensing properties of the nanostructured layers of semiconducting metal oxide materials. *Sensors and Actuators B: Chemical*, *170*, 148-157.

[20] Smith H.M. & Turner A.F. (1965) Vacuum deposited thin films using a ruby laser. *Applied Optics*, *4*(1), 147-148.

[21] Chrisey D.B. & Hubler G.K. (1994) Pulsed Laser Deposition of Thin Films, USA: John Wiley & Sons, Inc.

[22] Marcu A. & Viespe C. (2015) Laser-grown ZnO nanowires for room-temperature SAW-sensor applications. *Sensors and Actuators B: Chemical*, *208*, 1-6.

[23] Vanalakar S.A., Agawane G.L., Shin S.W., Suryawanshi M.P., Gurav K.V., Jeon K.S., ... & Kim J.H. (2015) A review on pulsed laser deposited CZTS thin films for solar cell applications. *Journal of Alloys and Compounds*, *619*, 109-121.

[24] Haider A.J., Shaker S.S. & Mohammed A.H. (2013) A study of morphological, optical and gas sensing properties for pure and Ag doped SnO_2 prepared by pulsed laser deposition (PLD). *Energy Procedia*, *36*, 776-787.

[25] Akiyama M., Tamaki J., Miura N. & Yamazoe N. (1991) WO_3-Based Semiconductor Sensor Highly Sensitive to NO and NO_2. *Chemistry Letters*, (9), 1611-1614.